HHS Public Access

Author manuscript

Nat Metab. Author manuscript; available in PMC 2025 May 01.

Published in final edited form as:

Nat Metab. 2024 November ; 6(11): 2187–2202. doi:10.1038/s42255-024-01143-3.

Brown Fat ATP-Citrate Lyase Links Carbohydrate Availability to Thermogenesis and Guards Against Metabolic Stress

Ekaterina D. Korobkina[1], **Camila Martinez Calejman**[1], **John A. Haley**[1], **Miranda E. Kelly**[2], **Huawei Li**[1], **Maria Gaughan**[1], **Qingbo Chen**[1], **Hannah L. Pepper**[3], **Hafsah Ahmad**[3], **Alexander Boucher**[1], **Shelagh M. Fluharty**[1], **Te-Yueh Lin**[1], **Anoushka Lotun**[1], **Jessica Peura**[4], **Sophie Trefely**[5,6], **Courtney R. Green**[7], **Paula Vo**[1], **Clay F. Semenkovich**[9], **Jason R. Pitarresi**[4,10], **Jessica B. Spinelli**[1], **Ozkan Aydemir**[1], **Christian M. Metallo**[7,8], **Matthew D. Lynes**[11], **Cholsoon Jang**[2], **Nathaniel W. Snyder**[3], **Kathryn E. Wellen**[5,6], **David A. Guertin**[1,10]

[1] Program in Molecular Medicine, University of Massachusetts Chan Medical School, Worcester, MA, USA

[2] Department of Biological Chemistry, University of California Irvine, Irvine, CA, USA

[3] Aging + Cardiovascular Discovery Center, Lewis Katz School of Medicine, Temple University, Philadelphia, PA, USA

[4] Division of Hematology-Oncology, Department of Medicine, University of Massachusetts Chan Medical School, Worcester, MA, USA

[5] Department of Cancer Biology, University of Pennsylvania Perelman School of Medicine, Philadelphia, PA, USA

[6] Abramson Family Cancer Research Institute, University of Pennsylvania Perelman School of Medicine, Philadelphia, PA, USA

[7] Department of Bioengineering, University of California, San Diego, La Jolla, USA

[8] Molecular and Cellular Biology Laboratory, The Salk Institute for Biological Studies, La Jolla, USA

[9] Division of Endocrinology, Metabolism and Lipid Research, Washington University School of Medicine, St. Louis, MO, USA

[10] Department of Molecular, Cell and Cancer Biology, University of Massachusetts Chan Medical School, Worcester, MA, USA

[11] MaineHealth Institute for Research, Scarborough, Maine, USA

Corresponding author: D. A. Guertin; David.Guertin@umassmed.edu.

Author contributions

Conceptualization: D.A.G., E.D.K., C.M.C., K.E.W.
Methodology: E.D.K., C.M.C., J.A.H., J.R.P., J.B.S., O.A, C.M.M, M.D.L., C.J, N.W.S.
Investigation: E.D.K., C.M.C., J.A.H, M.E.K., H.L., M.G., Q.C., H.L.P., H.A., A.B., S.M.F., T.Y.L., A.L., J.P., S.T., C.R.G., P.V., C.F.S., O.A., M.D.L.
Visualization: E.D.K., D.A.G.
Supervision: D.A.G., K.E.W., N.W.S. C.J.
Writing: E.D.K., D.A.G.

Competing interests

Authors have no competing interests.

Abstract

Brown Adipose Tissue (BAT) engages futile fatty acid synthesis-oxidation (FAS-FAO) cycling, the purpose of which has remained elusive. Here, we show that ATP-citrate lyase (ACLY), which generates acetyl-CoA for fatty acid synthesis, promotes thermogenesis by mitigating metabolic stress. Without ACLY, BAT overloads the TCA cycle, activates the integrated stress response (ISR), and suppresses thermogenesis. ACLY's role in preventing BAT stress becomes critical when mice are weaned onto a carbohydrate plentiful diet, while removing dietary carbohydrates prevents stress induction in ACLY-deficient BAT. ACLY loss also upregulates *fatty acid synthase (Fasn)*; yet while ISR activation is not caused by impaired fatty acid synthesis *per se*, deleting *Fasn* and *Acly* unlocks an alternative metabolic program that overcomes TCA cycle overload, prevents ISR activation, and rescues thermogenesis. Overall, we uncover a previously unappreciated role for ACLY in mitigating mitochondrial stress that links dietary carbohydrates to UCP1-dependent thermogenesis and provides fundamental insight into the FAS-FAO paradox in BAT.

Introduction

Brown adipose tissue (BAT) mediates non-shivering thermogenesis, an adaptive process by which mammals maintain body temperature in the cold. BAT thermogenesis is triggered by norepinephrine and mediated by uncoupling protein 1 (UCP1), an inner mitochondrial membrane protein that dissipates the electrochemical proton gradient to produce heat [1–4]. In humans, BAT is protective against cardiometabolic diseases and cancer [5,6], which may be attributable to its ability to expend energy from excess nutrients as heat and function as a source of beneficial hormones and metabolites [2,7,8,9]. Consequently, targeting BAT is under scrutiny as a therapeutic strategy against obesity and related metabolic diseases.

BAT thermogenesis is driven by fatty acid oxidation (FAO), which fuels the tricarboxylic acid (TCA) cycle and supports uncoupled respiration in mitochondria [1,10]. Paradoxically, BAT also increases cytosolic fatty acid synthesis resulting in a futile cycle[11–15]. In fact, BAT is one of the most lipogenic tissues in the body[12,16]. ATP-citrate lyase (ACLY) is the major source of cytosolic acetyl-CoA for *de novo* lipogenesis (DNL), the process of synthesizing lipids from non-lipid precursors such as glucose, while acyl-CoA synthetase short chain family member 2 (ACSS2) can provide an alternative source of acetyl-CoA from acetate under certain conditions[17,18]. During fatty acid synthesis, ACLY uses citrate generated by the TCA cycle and exported from mitochondria to synthesize acetyl-CoA, which is further processed by acetyl-CoA carboxylase (ACC1) and fatty acid synthase (FASN) into malonyl-CoA and C16:0 palmitate, respectively. BAT robustly upregulates both ACLY and ACSS2 in the cold, which coincides with increased glucose uptake and flux into DNL and acyl-carnitines, the latter transporting newly synthesized fatty acids back into mitochondria for oxidation [13–15,19–21]. Importantly, while the existence of this futile FAS-FAO cycling in BAT has been recognized for decades, its function has long remained elusive.

Results

BAT ACLY Loss Causes Tissue Whitening and Cold Intolerance

To investigate the role of ACLY and ACSS2 in BAT, we generated *Ucp1-Cre;Acly*$^{l/l}$ and *Ucp1-Cre;Acss2*$^{l/l}$ mice (hereafter *Acly*^{BATKO} and *Acss2*^{BATKO}, respectively) [Fig. 1A]. At the standard vivarium temperature of 22°C, mice have highly thermogenic BAT because they are below their thermoneutral zone [22]. Under these conditions, ACLY loss, confirmed by Western blot, causes profound BAT whitening in males that correlates with a 20% increase in tissue mass [Fig. 1B–D][23]. Total body weight and the mass of other tissues are unaffected [Ext. data Fig. 1A–C]. To evaluate the physiological relevance of these findings, we performed a cold challenge by exposing mice to a 4°C environment. While control mice maintain euthermia for up to 8 hours, which is the pre-determined experimental limit, *Acly*^{BATKO} mice rapidly become hypothermic at 4 hours requiring sacrifice when body temperature reached the low body temperature limit of 30°C, shown as per mouse temperature curves over time [Fig. 1E] and survival curves [Ext. data Fig. 1D]. Thermal camera imaging shows reduced heat dissipation from the interscapular skin surface of *Acly* mutants, the anatomical site of the largest BAT depot [Ext. data Fig. 1E]. Female mice showed similar results [Ext. data Fig. 2A–F]. In contrast, *Acss2*^{BATKO} mice showed no significant differences in any of these parameters [Fig. 1F–H, Ext. data Fig. 1F–J, Ext. data Fig. 2G–L]. These findings indicate a critical role for ACLY in BAT function.

Impaired Lipid Metabolism in *Acly*-deficient BAT

BAT whitening in the *Acly*^{BATKO} mice suggests altered FAO. Consistently, expression of *carnitine palmitoyltransferase 1b (Cpt1b*), c*arnitine palmitoyltransferase 2* (*Cpt2*), and several other FAO genes decrease in the mutant mice[Fig. 1I]. Lipid profiling further shows an increase in di- and triglycerides with longer and more desaturated fatty acyl chains [Ext. data Fig. 3 A–E] that is paralleled by increased in elongase (*Elovl6)* and desaturase (*Scd1*, *Scd5*) gene expression [Fig. 1J–K]. Despite triglyceride accumulation, regulators of triglyceride synthesis such as *diacylglycerol O-acyltransferase (Dgat1), Dgat2, and 1-acyl-sn-glycerol-3-phosphate acyltransferase alpha (Agapat1)* are decreased [Fig. 1K] suggesting reduced FAO rather than increase triglyceride synthesis causing BAT whitening. Consistently, *Acly*-mutant BAT also has reduced DNL [Ext. data Fig. 3 F–H], reduced glucose uptake (which fuels DNL) [Ext. data Fig. 3I], reduced *Glut4* (which encodes the insulin-regulated glucose transporter) [Ext. data Fig. 3J], and reduced expression of the fatty acid translocase *Cd36* and *lipoprotein lipase* (*Lpl*) genes that promote lipid uptake [Ext. data Fig. 3K] [23,24]. Overall, these data suggest reduced FAO is the major driver of BAT whitening.

An Impaired Mitochondria Network in *Acly*-deficient BAT

Active BAT has an extensive network of UCP1-containing mitochondria that are the main sites of FAO. Strikingly, the levels of UCP1 [Fig. 1D, 2A–B], the electron transport chain subunits NDUFB8, SDHB, UQCRC2, and MTCO1, (representing complexes I-IV) [Fig. 2A], and COQ9 (the main electron carrier in mice) [Fig. 2C] decrease in *Acly* mutant BAT indicating impaired uncoupling respiration. These deficiencies reflect a broader mitochondria defect as *Cycs* mRNA, which encodes Cytochrome C, decreases by 66% [Fig.

2D], and the mitochondrial to nuclear DNA ratio decreases by 65% in mutant tissue [Fig. 2E]. Consistently, phospholipids enriched in mitochondrial membranes such as cardiolipin (CL), phosphatidylcholine (PC), phosphatidylethanolamine (PE), phosphatidylinositol (PI), phosphatidylserine (PS), and phosphatidylglycerol (PG) are all lower in the mutant mice [Fig. 2F–G]. However, by electron microscopy, we observed no ultrastructural differences in individual mitochondria [Fig. 2H] suggesting a defect in mitochondria biogenesis or maintenance.

The Thermogenic Gene Program Requires ACLY

A well-defined thermogenic gene program drives mitochondria biogenesis and metabolic programming in BAT[25]. In *Acly*-deleted BAT, *Ppargc1a (Pgc1α)* and *Ppargc1b (Pgc1 β)*—the master transcriptional controllers of mitochondrial biogenesis—decrease by more than 50% while the related *Pprc1* (*Prc)* gene is unchanged [Fig. 2I]. Similarly, *Esrra (Errα)*, *Esrrβ (Errβ),* and *Esrrγ (Errγ)*, *Pparα* and *Pparγ*, and the *Ebf1*, *Ebf2,* and *Zfp516* genes, which cooperate with *Pgc1α/β*, all decrease in mutant BAT [26,27]. Notably, ACLY knockdown also decreases UCP1, PPARg, PGC1a, and respiratory chain markers *in vitro* [Ext. data Fig. 4A, E], which correlates with impaired oxygen consumption rate (OCR) and extra cellular acidification rate (ECAR) in this context [Ext. data Fig. 4B–C]. Moreover, ACLY knockdown has no effect on the mitochondria to nuclear DNA ratio [Ext. data Fig. 4D] consistent with mitochondria number reduction being part of the adaptative response to *Acly* loss. Notably, we did not observe changes in bulk histone acetylation on H3K9, H3K14, or H3K27 in ACLY knockdown cells [Ext. data Fig. 4F] or in brown adipocytes treated with an ACLY inhibitor (BMS-303141) [Ext. data Fig. 4G]. Overall, these data identify ACLY as a positive regulator of the core thermogenic gene program.

Beige Adipocyte Formation Also Requires ACLY

Prolonged severe cold exposure induces brown-like adipocytes called beige or brite adipocytes in subcutaneous white adipose tissue (WAT), a process called WAT browning [2,4]. To test whether ACLY is also required for WAT browning, we adapted *Adiponectin-Cre;Acly (Acly*^{FATKO}) mice, which lack *Acly* in all adipocytes, to a 6°C environment for 4 weeks. While this causes extensive SAT browning in controls [Fig. 3A], the *Acly*^{FATKO} mice were devoid of brite/beige adipocytes indicated by the absence of multilocular adipocytes [Fig. 3A], low expression of UCP1 mRNA and protein and respiratory complex subunit levels [Fig. 3B–C], reduced mitochondria to nuclear DNA ratio [Fig. 3D], and low expression of thermogenic genes including *Cidea*, *Cycs*, *Ppargc1a*, *Ppargc1b*, *Essra, Esrrg*, and *Ebf2* [Fig. 3E]. Thus, ACLY is also required for WAT browning.

Induced ACLY loss triggers the Integrated Stress Response

To investigate the mechanism by which ACLY loss impairs thermogenesis, we generated inducible *Ucp1-CreER;Acly* (*Acly*^{BATiKO}) mice to assess the impact of more abrupt *Acly* loss. Inducing *Acly* deletion initiates BAT whitening and UCP1 depletion within two weeks of CreER activation [Fig. 4A–B, Ext. data Fig. 5A–C]. We performed bulk RNA-sequencing following induced *Acly* loss, which uncovered 1114 and 560 genes that increase or decrease [Fig. 4C–F], respectively upon induced *Acly* loss [FDR<0.05, log2(Fold Change)<−1, log2(Fold Change)>1]. Notably among the downregulated genes

by Gene Ontology were those encoding mitochondria and respiratory chain factors and regulators of lipid metabolism [Fig. 4C, 4D, Ext. data Fig. 5D], which is consistent with RT-PCR and Western results from the congenital *Ucp1-Cre;Acly* knockout mice. Conversely, highly overrepresented among the upregulated genes are markers of inflammation [Fig. 4E], suggesting metabolic stress.

Consistent with metabolic stress, we also identified genes targeted by the integrated stress response (ISR) as significantly upregulated by induced *Acly* loss [Fig. 4F][28]. The ISR is a signaling network that reestablishes homeostasis in response to metabolic stress[29–31]. The ISR has also been implicated in suppressing thermogenesis[32]. Consistently, critical markers of ISR activation including EIF2a phosphorylation and ATF4 expression are highly upregulated following induced *Acly* deletion [Fig. 4B, Ext. data Fig. 5D]. Activation of the ISR is also accompanied by altered mitochondria quality control indicated by increased p62 and its target, the NRF2 stress responsive transcription factor 2 [Ext. data Fig. 5E], increased LC3-II and Parking indicating altered mitophagy[33][Ext. data Fig. 5E], and decreased OPA1 and DRP indicating altered fusion-fission dynamics[34][Ext. data Fig. 5E]. These data suggest that induced *Acly* deletion causes an abrupt metabolic stress that triggers the ISR and mitochondria quality control pathways that cooperatively shutdown thermogenesis and reestablish metabolic homeostasis.

ACLY's Role in Mitigating Stress is Linked to Dietary Carbohydrates

During weaning, when mice switch from a lipid-rich milk diet to a solid carbohydrate-plentiful diet, we noted robust upregulation of ACLY, ACC, and FASN expression in BAT coincident with increased DNL; ACSS2 level was unchanged [Fig. 5A][12]. This suggested BAT ACLY expression is linked to dietary carbohydrates, which led us to ask whether ACLY's role in thermogenesis is diet dependent. This is indeed the case; $Acly^{BATKO}$ mice, which lack ACLY in BAT from birth, begin developing whitened BAT only after weaning [Fig. 5B]. Comparing BAT from control and $Acly^{BATKO}$ littermates that are pre-weaned (2-weeks-old) or post-weaned (4-week-old) shows ISR activation (i.e. increased p-Eif2a/Eif2a, ATF4/*Atf4*, *Ddit3,Trib3*), UCP1/*ucp1* depletion, and reduced mitochondria number only after weaning [Fig. 5C–F; Ext. data Fig. 6A–B], coinciding with the dietary switch. We additional observe compensatory upregulation of *acss2*/ACSS2 and *fasn*/FASN only upon weaning, which correlates with increased ChREBPb expression [Ext. data Fig. 6C–F]. Remarkably, when weaned onto a carbohydrate free, there was no DNL pathway induction, tissue whitening, or ISR activation [Fig. 5G–N]. Thus, ACLY's critical role in mitigating stress is diet dependent.

We also noted that *Ucp1* and mtDNA are higher in control BAT when mice are weaned onto the carbohydrate plentiful diet compared to the carbohydrate free diet [Fig. 5M, 5N]. Moreover, *Acly* deletion results in no significant difference in mtDNA or *Ucp1* levels between control and mutant tissue on the carbohydrate-free diet [Fig. 5M, 5N] although UCP1 protein remained slightly lower in the mutant tissue on the carbohydrate-free diet [Fig. 5G]. This further suggests a greater dependency on ACLY for UCP1-dependent thermogenesis in the carbohydrate plentiful diet vs. the carbohydrate-free diet. Interestingly, mice weaned onto the carbohydrate-free diet increases creatine kinase B (CKB) expression,

which drives the futile creatine cycle [Fig. 5G][35]suggesting diet may alter the balance between UCP1-depenendent and independent thermogenesis pathways. Overall, these findings support a model in which ACLY's critical role in mitigating BAT stress is linked to dietary carbohydrates, which provide the substrate for ACLY activity (i.e. mitochondria exported citrate) and a signal linking expression of ACLY and other DNL enzymes to a UCP1-high thermogenic program.

ACLY Prevents TCA Cycle Overload During Thermogenesis

To begin unraveling the cause of metabolic stress in ACLY-deficient BAT, we first performed acyl-CoA profiling using *Acly*^{BATKO} mice. Both acetyl-CoA and malonyl-CoA levels are greatly reduced in congenital *Acly* knockout BAT [Fig 6A, 6B]. Major mitochondrial acyl-CoA species such as CoASH, Butyryl-CoA, and Succinyl-CoA also decrease substantially [Fig 6C–E]. The drop in malonyl-CoA, which is mainly cytosolic, further suggests little to no flux into DNL in the *Acly* mutant BAT, which we functionally confirm in a later figure. On the other hand, HMG-CoA levels trend lower but do not differ significantly between control and mutant [Fig. 6F] suggesting ACLY-independent sources of acetyl-CoA may support the mevalonate pathway under these conditions.

Next, we performed *in vivo* ^{13}C-glucose isotope tracing experiments. To capture early metabolic changes linked to ISR activation, we delivered the tracer to control and *Acly*^{BATKO} mice at 4.5weeks of age, shortly after weaning onto the carbohydrate plentiful diet, thereby coinciding with the early onset of BAT whitening. We then collected BAT samples at 15- and 30-minutes post tracer delivery [Fig. 6G–H, Ext. data Fig. 7A–B]. This revealed a substantial increase in the labeling of TCA cycle metabolites (i.e. citrate, oxoglutarate, fumarate, and malate) at both 15 and 30 minutes [Fig. 6I–J] suggesting TCA cycle overload. Consistently, a significant fraction of glucose is also diverted to lactate [Fig 6I–J]. In addition, glucose labeling is decreased suggesting an increase in glycolytic flux in the early stages of *Acly* dependency [Fig 6I–J]. As TCA cycle overload can stimulate the ISR[28,36], these data suggest a mechanism by which ACLY mitigates BAT metabolic stress by balancing TCA cycle load during thermogenesis.

BAT *Acly;Fasn* Loss Rescues Thermogenesis Independent of DNL

We considered the possibility that a defect in fatty acid synthesis downstream of *Acly* loss could cause BAT whitening, and tested this by deleting BAT *Fasn;* however, *Fasn* deletion did not trigger whitening [Ext. Data Fig. 8A–B], reduce UCP1 [Ext. Data Fig. 8C] or cause cold intolerance [Ext. Data Fig. 8D] in males or females [37,38]. In contrast, UCP1 levels are higher in male *Fasn*^{BATKO} mice. BAT mtDNA levels are also unaffected in the *Fasn*^{BATKO} mice and CoQ levels are normal [Ext. Data Fig. 8E, F]. These observations support the notion that BAT whitening upon *Acly* loss is caused by mitochondrial stress rather than a downstream defect in fatty acid synthesis. Nevertheless, throughout this study, we noted that *Acly* loss causes a strong compensatory upregulation of FASN [Fig. 1D, Fig. 4B, Fig. 5C, Fig. 5G, Fig. 6H][17,23]. This led us to ask whether aberrant FASN expression might contribute to thermogenesis suppression.

To address this question, we generated BAT-specific *Acly;Fasn* double knockout (DKO) mice using both *Ucp1-Cre* and *Ucp1-CreER*. We also generated BAT-specific *Acly;Acss2* DKOs for comparison because *Acly* loss also causes compensatory ACSS2 upregulation [Fig. 1D, Fig. 4B, Fig. 5C, Fig. 5G, Fig. 6H]. DKO of *Acss2* had no effect; that is the *Acly* single KO phenotype predominates [Ext. Data Fig 9]. In remarkable contrast, *Acly;Fasn* DKO rescues *Acly* loss. For example, $Acly;Fasn^{BATDKO}$ mice on a carbohydrate plentiful diet have normal BAT morphology [Fig. 7A, Ext. Data Fig. 10A–B], tissue mass [Fig. 7B], UCP1 expression [Fig. 7C], mtDNA levels [Fig. 7D], CoQ levels [Fig. 7E], and thermogenic gene expression [Fig. 7F]. $Acly;Fasn^{BATDKO}$ mice also outperform $Acly^{BATKO}$ mice in a cold challenge [Fig. 7G]. Interestingly, *Acly, Fasn*, and both *Acly;Acss2* and *Acly;Fasn* deleted BAT show equal impairment of DNL by heavy water labeling, a functional measure of DNL [Fig. 7H, Ext. Data Fig. 10C]. Because FASN is essential for DNL, this indicates (1) that *Acly* is the major source of lipogenic acetyl-CoA; (2) that there is no compensatory acetyl-CoA production via ACSS2 under these conditions; and (3) that doubly deleting *Fasn* may rescue *Acly* loss by a mechanism independent of DNL *per se*.

BAT *Acly;Fasn* Loss Rebalances Thermogenic Metabolism

BAT Acetyl-CoA levels are also normalized in the *Acly;Fasn* DKO consistent with acetyl-CoA levels mainly reflecting mitochondrily derived acetyl-CoA rather than flux into DNL [Fig. 6K]. Similarly, the DKO also normalizes CoASH levels [Fig. 6M], and HMG-CoA levels are also unchanged [Fig. 6P]. However, malonyl-CoA levels, which substantially decrease in the *Acly* KO, increase by more than 4-fold over control in the DKO [Fig 6L]. This was surprising given that *Acly* loss inhibits DNL to the same extent as deleting *Fasn* alone or in the *Acly;Fasn* DKO [Fig 7H]. Thus, FASN overexpression in *Acly* mutant BAT appears to restrict access to an alternative source of Acetyl-CoA that can be used to make Malonyl-CoA.

Increased malonyl-CoA is well known to allosterically inhibit CPT1, the mitochondrial long-chain fatty acid transporter, which would reduce carbon flux from fatty acid oxidation into the TCA cycle. Consistent with this notion, ^{13}C-Glucose tracing shows reduced flux into most TCA cycle metabolites and no flux into lactate in the *Acly;Fasn* DKO compared to the *Acly* single KO BAT [Fig. 6Q–R]. Interestingly, there is also elevated flux into glycerol-3-phosphate and 3-phosphoglycerate at 15 minutes only in the DKO hinting at additional diversion of carbon away from mitochondria [Fig. 6Q–R]. Succinyl-CoA and Butyryl are also substantially elevated over control in the DKO [Fig. 6N, 6O] further suggesting alternative metabolic routes. Taken together, these data suggest that *Fasn* double deletion rescues *Acly* loss by rebalancing how carbons enter the mitochondria and/or the TCA cycle during thermogenesis.

BAT *Acly;Fasn* Double Knockout Prevents ISR activation.

Finally, we asked whether the rebalancing of TCA cycle load in the *Acly;Fasn* DKO prevents activation of the ISR. This was indeed the case; we found that inducing BAT *Acly;Fasn* double knockout not only prevents tissue whitening and UCP1 depletion [Fig. 7I, Ext. Data Fig. 10D–F], but prevents the upregulation of phospho- and total Eif2a and ATF4 [Fig. 7I]. Moreover, bulk RNA-sequencing shows that $Acly;Fasn^{BATDKO}$ BAT is more like

control than the *Acly*-deficient BAT [Ext. Data Fig. 10G], and it completely suppresses ISR gene activation [Fig. 7J] as well as the inflammation gene signature [Ext. Data Fig. 10H]. Thus, doubly deleting *Fasn* and *Acly* not only rebalances thermogenic metabolism, but also completely prevents activation of the ISR.

Discussion

Futile FAS-FAO cycling in BAT (i.e. *de novo* synthesizing lipids form glucose for immediate catabolism) has been recognized for decades, but its function has long been unclear. Trayhurn proposed that FAS-FAO cycling could contribute to heat dissipation in BAT through futile ATP hydrolysis[12], marking an early reference to UCP1-independent thermogenesis pathways. Here, we add additional insight into this paradox by providing evidence that FAS-FAO cycling defends against metabolic stress. We propose the following model [Fig. 8]: Increased FAS-FAO cycling is a homeostatic response that mitigates metabolic stress by preventing TCA cycle overload and maintaining UCP1, specifically when the diet is high in carbohydrates. Without ACLY, the TCA cycle overloads, the ISR is activated, and the thermogenic program shuts down. We also discovered an unexpected role for FASN in this process. Upon ACLY loss, FASN expression increases and contributes to thermogenesis suppression such that double deletion of FASN leads to an alternative metabolic program that rebalances TCA cycle load. This rebalancing is associated with elevated malonyl-CoA levels, known to reduce FAO flux into the TCA cycle, and altered glucose utilization. Surprisingly, this rebalancing does not coincide with changes in DNL. Future isotope tracing and functional studies should further resolve this metabolic rewiring, which is important because recent studies suggest the existence of DNL-high and DNL-low thermogenic adipocytes [21,39], the significance of which is enigmatic.

Interestingly, Fasn deletion in subcutaneous white adipocytes induces the thermogenic program at room temperature in conjunction with increased malonyl-CoA levels, regardless of whether Acly is present or deleted in the subcutaneous fat, and genetic analysis suggests that decreased palmitate levels rather than increased malonyl-CoA may be the important metabolite signal in this context[40]. However, the role of FASN in brown vs. beige adipocytes remains unclear and needs additional study.

BAT is highly insulin sensitive in mildly cold mice; thus, insulin is likely an important modulator of ACLYs ability to “pull” citrate from the TCA cycle, as suggested by previous adipocyte metabolic flux studies[41]. This would be an elegant mechanism linking systemic glucose availability to thermogenesis during the energetically intense process of non-shivering thermogenesis, and why lowering the glycemic index by removing glucose from the diet may abrogate this link. It is alternatively possible that the high fat content of the carbohydrate free diet somehow promotes ACLY-independent thermogenesis, for example by suppressing FASN expression. It will also be interesting to examine the role of ACLY in a more severely cold environment as BAT insulin signaling drops at colder temperatures and the transcriptional regulation of glycolysis and GLUT1-mediated transport predominates under these more extreme cold conditions[14,15,42].

Using an inducible knockout approach to achieve abrupt tissue specific ACLY loss, we show rapid activation of the ISR. Our observation of an overloaded TCA cycle is consistent with this response as this would increase the mitochondrial NADH/NAD+ ratio, a known stimulus of the ISR [28,36]. Attenuation of UCP1 expression might also contribute to ISR activation and/or TCA overload, possibly resulting in a feedback loop that exacerbates metabolic imbalances[43]. While our *in vitro* studies suggest ISR activation occurs before UCP1 decline, we could not temporally uncouple ISR activation from UCP1 attenuation *in vivo* leaving open the possibility that ACLY could regulate UCP1 levels by an additional route. CoQ9 depletion has also been linked to ISR activation[44]; however, the precursor HMG-CoA did not significantly decrease in *Acly*-deleted BAT. Nevertheless, given the broad roles of acetyl-CoA in metabolism, other pathways could also contribute to ISR activation upon acute ACLY loss. Interestingly, we also observed increased lipid elongation and desaturation in *Acly*-deleted BAT. This was notable considering a recent report that synthesis of highly unsaturated fatty acids can occur through an adaptative desaturase response to cytosolic NAD^+ depletion[45]. The by-product of cytosolic citrate cleavage by ACLY is oxaloacetate, which is converted to malate by cytosolic malate dehydrogenase in a reaction that regenerates NAD^+. This pool of oxaloacetate is presumably depleted upon *Acly* deletion, raising the intriguing possibility that a cytosolic redox imbalance caused by decreased oxaloacetate production might contribute to metabolic stress and/or BAT whitening upon *Acly* loss. Future studies aimed at resolving compartmentalized metabolite levels should address this.

Interest in UCP1-independent heat generating futile cycles in brown and beige fat is gaining momentum[46–48]. While such cycles may contribute to thermogenesis, our data suggest futile FAS-FAO cycling may have coevolved with UCP1-dependent thermogenesis to provide additional advantages, such as preventing substrate overaccumulation. Futile cycles might also generate signaling metabolites that help maintain metabolic efficiency. In humans, the amount and activity of brown fat correlates with resistance to cardiometabolic diseases [49,50]; on the contrary, adipocyte energy wasting contributes to cancer associated cachexia [51,52]. Thus, understanding and pharmacologically modulating thermogenic adipocytes and/or futile cycling has considerable translational implications.

Materials and Methods

Mice

C57BL/6J mice (JAX stock 000664) were obtained from Jackson Laboratory and were the genetic background of the mice used in this study. *Ucp1-Cre* mice (JAX-024670) and *Adiponectin-Cre* were provided by Dr. Evan Rosen, $Acly^{l/l}$ mice were generated by Dr. Kathryn Wellen (JAX-043555), $Fasn^{l/l}$ mice were generated by Dr. Clay Semenkovich, $Acss2^{l/l}$ mice were generated at the University of Iowa for this study, *UCP1-Cre-Er* mice were obtained from Dr. Christian Wolfrum. Following mice were generate by crossing in the lab: *Ucp1-Cre-*$Acly^{l/l}$ (hereafter $Acly^{BATKO}$ mice), *Ucp1-Cre Acss2*$^{l/l}$, *Ucp1-Cre Acly,Acss2*$^{l/l}$, *Ucp1-Cre Fasn*$^{l/l}$, *Ucp1-Cre-Acly,Fasn*$^{l/l}$, *Ucp1-Cre-ER Acly*$^{l/l}$, *Ucp1-Cre-ER Acly,Fasn*$^{l/l}$, *Adiponectin-Cre Acly*$^{l/l}$(hereafter $Acly^{FATKO}$ mice). Mice were housed in the UMass Chan Animal Medicine facilities in a room set at 22±1°C in 50±20% humidity,

under daily 12h light/dark cycles, mice had free access to food (Prolab Isopro® RMH 3000) and water for all the experiments unless otherwise stated. For all experiments, mice were randomly assigned to treatments and randomized during dissections. All dissections were blinded, noting that some phenotypes are clear. All experiments were approved and performed in accordance with University of Massachusetts Chan Medical School Institutional Animal Care and Use Committee (IACUC).

Acute Cold Challenge Experiments

For acute cold challenge experiments, 8–12-week-old mice and littermate controls (both males and females) were transferred between 8–10am to prechilled cages in a 4°C cold room with free access to pre-chilled water and without access to food. Mice were placed two per cage. Rectal temperature was measured hourly using a rectal probe (RET-3, ThermoWorks). BAT temperature was obtained using an infrared thermal camera (FLIR T420) in lightly anesthetized mice at the end of the acute cold challenge and analyzed with FLIR Tools.

Cold Adaptation

For cold adaptation experiments, 6-week-old mice and littermate control (males) were housed at 6°C cold chamber for four weeks with free access to food and water. Mice were housed two per cage.

Carbohydrate Free Diet

For the diet experiment 3-week-old mice *Ucp1-Cre Acly*$^{fl/fl}$ and their littermate controls were weaned to a Matched Control Diet (Research Diets D10070802i) or Carbohydrate Free Diet (Research Diets D10070801i). Animals remained on the diet for 3 weeks.

Tamoxifen Injections for Conditional Kock Out

Tamoxifen (Sigma, T5648) was dissolved in sunflower oil (Spectrum, S1929) for final concentration of 1mg tamoxifen/100uL oil. 100uL of tamoxifen was injected intraperitoneally into each mouse on Day 0, Day 2 and Day 4. Tissues were collected on Day 14, two weeks after first injection.

Brown Adipocyte Differentiation

Brown preadipocytes were isolated from postnatal day 1 neonates and immortalized with pBabe-SV40 large T antigen in accordance with standard protocol[53], and as described previously[54]. The sex of the neonates was not determined.

Cells were maintained in Dulbecco's Modified Eagle Medium (DMEM) supplemented with 10% fetal bovine serum (FBS), 1% antibiotics, and incubated at 37°C and a 5% CO2. For differentiation, cells were plated (D0) with Differentiation Media: DMEM supplemented with 10% FBS, 1% antibiotics, 20 nM insulin and 1 nM T3. Once cells were confluent they were induced (D2) with Differentiation Media supplemented with 0.125mM of indomethacin, 2 mg/ml dexamethasone and 0.5 mM 3-isobutyl-1-methylxanthine for 2 days. After 2 days media was replaced back to Differentiation Media and changed every 2 days until maturation (D8).

siRNA Cell Transfection

Non-targeting control (D-001206–14-05) siRNA and *siAcly* (M-040092–00-0005) were obtained from Horizon Discovery. Differentiated brown adipocytes (D8) were reverse transfected[19]. 25 nM siRNA was reverse transfected using Lipofectamine RNAiMax (Thermo Fisher, 13778150) in accordance with manufacturer's instructions. 600,000 cells/well was used for 12-well plates. Fresh media was added 2 days after transfection, and cells were collected 4 days after transfection.

Acly Inhibitor

Mature adipocytes, see section Brown Adipocyte Differentiation, were treated with Acly inhibitor (BMS-303141) at 30uM for various times.

Chromatin Extraction

Mature adipocytes were treated with siRNA or Acly inhibitor. Cells were lysed with Lysis buffer for 20 minutes on ice (10mM HEPES pH7.4, 10mM KCl, 0.05% NP-40, including a protease (Biotool Cat. Number B14011) and phosphatase inhibitor cocktail (Sigma Cat. Number P5726). Lysate was centrifuged at 21300xg for 10 minutes at 4°C. Supernatant was removed and chromatin was extracted from nuclear pellet with 0.2N HCl and neutralized with an equal volume of 1M Tris-HCl pH8 in a fresh tube. Histone samples were run at 5ug per sample.

Tissue Collection and Processing

Tissues for western blot and qPCR were placed into Eppendorf tubes and snap-frozen in liquid nitrogen.

For metabolite measurements, tissues were snap-frozen using a liquid nitrogen-cooled Wollenburg clamp. Tissues then were transferred into 2mL Eppendorf tubes with a pre-cooled 5mm metal bead. Tissues were homogenized using cryomill (Retsch, Newtown, PA), at 25 Hz for 1–2 minutes. Tissue powder was weighed out into pre-cooled Eppendorf tubes.

Seahorse

Cellular mitochondrial respiration rate (OCR) and extracellular acidification rate (ECAR) were measured using a Seahorse XFe96 Analyzer (Agilent). Mature brown adipocytes were plated and transfected in a Seahorse 96-well plate using siRNA. The assay was run 4 days after transfection. For the mitochondrial stress test, the following drug concentrations were used: 2.5 μM oligomycin, 0.5 μM FCCP, and 0.5 μM rotenone and antimycin A. Measurements were conducted with 3 measurement cycles and 3-min measurements. Hoechst 33342 (4 μM) was injected during the final injection to allow normalization to cell number using the CytationV (Agilent). Maximal OCR was calculated by subtracting baseline from the maximal FCCP value. Maximal glycolysis ECAR was calculated by subtracting baseline from maximal Oligomycin response. Wave (Agilent) was used for data acquisition.

Tissue Histology

Tissue pieces were fixed in 10% formalin overnight at 4°C. Tissues were embedded, sectioned and stained with Hematoxylin and Eosin (H&E) by the UMass Chan Morphology Core Facility. Images were acquired at 20x using Zeiss Axio Scan.Z1. Images were processed with Zeiss Zen Blue Software 3.7.

For Electron Microscopy tissues were embedded, sectioned, and imaged by the UMass Chan Electron Microscopy Facility.

Immunofluorescent Staining

For immunofluorescent staining, tissue sections were deparaffinized in Xylene, rehydrated, and antigen retrieval was performed with R-Buffer A (Electron Microscopy Sciences 62706–10). Slides were blocked and permeabilized for 1h at room temperature with 5% donkey serum in 0.3% PBS-Triton X. Slides were left in primary UCP1 antibody in 5% donkey serum in 0.3% PBS-Triton X, overnight at 4°C. Slides were washed in PBS-Tween (0.1%) twice for 5 minutes each prior to adding secondary. Slides were left in secondary antibody in 5% donkey serum in 0.3% PBS-Triton X, for 1h at room temperature and then washed again in PBS-Tween (0.1%) twice for 5 minutes each. Slides were mounted in Fluoromount-G™ Mounting Medium with DAPI (Invitrogen 00–4959-52). Imaging was completed on a Leica Thunder Tissue Imager and analyzed on QuPath.

Western Blot Analysis

For cell analysis, cells were washed with PBS and lysed in lysis buffer (1% Triton X-100, 50 mM HEPES at pH 7.4, 150 mM NaCl, 2 mM EDTA and 1% glycerol, protease and phosphatase inhibitors).

For tissue analysis, tissues were placed into 2mL Microcentrifuge tubes (USA scientific) with 5mm metal beads and RIPA lysis buffer containing 150 mM NaCl, 50mM HEPES pH 7.4, 2mM EDTA, 10mM glycerol, 1% TritonX-100, 0.5% deoxycholate, 0.1% SDS, including a protease (Biotool Cat. Number B14011) and phosphatase inhibitor cocktail (Sigma Cat. Number P5726). Tissues were lysed using TissueLyserII (Qiagen). Samples were run on SDS-Polyacrylamide gels, transferred to PVDF membrane and analyzed.

Mitochondria/Nuclear DNA Quantification

Protocol was modified from [55]. DNA was isolated using Universal Genomic DNA Kit (CWBio#CW2298M). qPCR was ran using following primers: ND1 and HK2 primers (sequences provided in supplement), for method see section Gene Expression Analysis.

Gene Expression Analysis

For cells, RNA was isolated directly with RNeasy Mini Kit (Qiagen). For tissues, RNA was isolated with Qiazol (Qiagen) and RNeasy Mini Kit (Qiagen). For cDNA prep, 1ug of RNA was reverse transcribed to cDNA using a High Capacity cDNA kit (#4368814, Applied Biosystems). qPCR was run with 10uL reactions with SYBR Green PCR master mix (CWBio#CW0955) on StepOnePlus Real-Time PCR System machine (Applied

Biosystems). Data analyzed as previously reported[56]. No data was excluded unless sample had poor amplification curve or was determined to be an outlier by ROUT test.

In vivo glucose uptake assays

3H-deoxyglucose ([1,2–3H(N)]-Deoxy-D-glucose) was used to evaluate glucose uptake into BAT, WAT, muscle and liver as previously described in [42]. Briefly, mixture of 3H-DOG (170 μCi/Kg) and unlabeled glucose (1g/Kg) was prepared as solutions in normal saline (0.9 % NaCl). Mice were fed the 3H-DOG/glucose mixture solution (10 μL/g body weight) through oral gavage using plastic feeding tube (Instech Laboratories, Plymouth meeting, MA) just before placing them at 4C. Half an hour following the gavage, organs and blood from anesthetized mice were harvested. Nutrient uptake data is expressed as the percentage of injected dose of [3H] per 1000 microgram of protein. Specific fractional uptakes of 3H-DOG were determined using a scintillation counter (liquid scintillation analyzer Tri-Carb 2900TR, PerkinElmer, Montreal, QC, Canada).

D2O labeling

Figure 3: Experiments were carried out as previously described in[57]. Briefly, twenty-four hours prior to termination, mice were intraperitoneally injected with 0.035 mL/g body weight 0.9% NaCl D2O (Sigma, 151882) and drinking water was replaced with 8% D2O enriched water.

Figure 6: Twenty-four hours prior to termination, mice were intraperitoneally injected with 300uL of 0.9% NaCl D2O (Sigma, 151882) and drinking water was replaced with 8% D2O water. Tissues were harvested see section Tissue Collection and Processing. Extraction was modified from [58]. 20mg of cryomilled tissue was extracted with 80% methanol:water. Samples were sonicated, centrifuged at 13000xg for 10minutes at 4°C. Pellet was resuspended in 1mL Chloroform: Methanol (2:1) and phase separated with 300uL of 0.9% NaCl. The nonpolar phase was then saponified and methylated with Boron Trifluoride at 95°C for 1 hour. 10 nM heptadecanoic acid was used as an internal standard. Samples were run as a 20:1 split on an 8890 GC system coupled to a 5977B single quadruple mass spectrometer (Agilent Technologies). The settings are as follows: GC inlet 280°C, transfer line 280°C, MS source 230°C MS Quad 150°C. An HP-5MS capillary column (30 m length, 250 μm diameter, 0.25 μm film thickness). Agilent MassHunter MS Quantitative Analysis software was used for analysis. ISOCOR was used to account for natural isotope abundances.

LC-MS/MS CoQ Measurements

Tissues were harvested see section Tissue Collection and Processing. 15–20mg of cryomilled tissue was weighed out into new tubes for further processing. Samples were vortexed in 450uL of 100% LC-MS grade ethanol (Sigma) for 10min at 4C. 900uL of 100% LC-MS grade hexane was added to each tube and vortexed for 10min at 4C. Samples were centrifuged at 21,300g at 4C for 10 minutes. The top layer (hexane) was transferred to a new tube and dried down with Refrigerated CentriVap Benchtop Vacuum Concentrator connected to a CentriVap-105 Cold Trap (Labconco). Pellet was used for protein quantification, using

Pierce BCA Protein Assay Kit (Life Technologies). Samples were resuspended to (20ug/uL) using protein concentrations.

For the analysis, a Q-Exactive orbitrap mass spectrometer with an Ion Max source and HESI II probe attached to a Vanquish Horizon UHLPC system was used. 2 µL of sample was injected and run on a Luna 3 µm PFP(2) 100 Å, 100 × 2 mm analytical column (Phenomenex). The column oven was set to 25°C and autosampler was set to 4°C. Buffer A was comprised of water containing 0.1% formic acid while Buffer B was compromised of acetonitrile containing 0.1% formic acid. The liquid chromatography settings were set at a flow rate of 0.5 mL/min with 70% Buffer B for 3 minutes, then increased to 98% Buffer over 0.25 minutes and held at 98% Buffer B for 1.75 minutes. Buffer B was then increased to 99% over the span of 1 minute and held at 99% Buffer B for 2.75 minutes. Buffer B was then dropped back down to 70% over the span of 1.75 minutes and held at 70% for the two minutes. The mass spectrometry scans were done in full scan (600–1000 m/z), positive mode with the spray voltage set to 4.0 kV, heated capillary to 320°C, HESI probe at 30°C, sheath gas flow at 40 units, auxiliary gas at 15 units, and sweep gas flow at 1 unit. The resolution of scan was set to 17,500, AGC target to 3×106, and maximum injection time at 250 msec.

TraceFinder 5.1 (ThermoFisher) was used for data analysis. Peaks were integrated using a strict 5 ppm mass tolerance and attention to the retention times as determined by purified standards of the respective metabolites. CoQ species measured: sum Ubiquinone 9 and Ubiquinol 9.

Lipidomics

10–20 mg of adipose tissue was transferred to an OMNI bead tube with 0.5 mL cold MeOH (−20°C) and was homogenized for 1.5 min at 4 °C using the OMNI Cryo Bead Ruptor 24 (OMNI international, Inc., Kennesaw, GA). An aliquot of the homogenate was taken for the protein analysis using BCA assay and 1 mg of sample based on protein concentration was added to internal standards and 4 ml chloroform:methanol (1:1, v/v) for the extraction. Lipid extracts were dried under nitrogen and reconstituted in 400 µl chloroform:methanol (1:1, v/v). Samples were flushed with nitrogen and stored at −20°C.

The concentrated sample was diluted 50× in isopropanol:methanol: acetonitrile:H2O (3:3:3:1, by vol.) with 2 mM ammonium acetate. The delivery of the solution to the SCIEX TripleTOF 5600+ (Sciex, Framingham, MA, USA) was either carried out using an Ekspert microLC 200 system with the flow rate at 6 µL/min on a customized loop. The parameters of mass spectrometer were optimized, and the samples were analyzed automatically using a data-independent analysis strategy, allowing for MS/MSALL high resolution and high mass accuracy [59,60].

Acyl-CoA Measurements

Acyl-CoAs were measured by liquid chromatography-high resolution mass spectrometry as previously described [61]. Aliquots of pre-weighed tissue of approximately 20 mg were spiked with 0.1 mL of $^{13}C_3{}^{15}N_1$-acyl-CoA internal standard prepared as previously described [62] and 0.9 mL of 10% (w/v) trichloroacetic acid in water. Samples were homogenized by using

a probe tip sonicator in 0.5 second pulses 30 times then centrifuged at 17,000 × g for 10 min at 4°C. Calibration curves were prepared from commercially available acyl-CoA standards (Sigma Aldrich). Calibration curve samples were also subjected to sonication and extraction in the same manner as the experimental samples to account for matrix effects, sample losses, and analyte stability. Samples and standards were purified by solid phase extraction (SPE) cartridges (Oasis HLB 10 mg) that were conditioned with 1 mL of methanol and 1 mL of water. Acid-extracted supernatants were loaded onto the cartridges and washed with 1 mL of water. Acyl-CoA metabolites were eluted with 1 mL of 25 mM ammonium acetate in methanol and dried under nitrogen. Samples were resuspended in 50 μL of 5% (w/v) 5-Sulfosalicyilic acid and 10 μL injections were analyzed on an Ultimate 3000 UHPLC using a Waters HSS T3 2.1×100mm 3.5 μm column coupled to a Q Exactive Plus. The analysts were blinded to sample identity during processing and quantification.

In Vivo Glucose Tracing

Experiment was performed as previously described[15].

Sample Collection: 4-week-old mice *Ucp1-Cre-Acly*$^{fl/fl}$, *Ucp1-Cre-Acly/Fasn*$^{fl/fl}$ and matched controls were used for this experiment. Prior to start of the experiment, tail blood was collected for 0-minute time point. Mice were gavaged (10uL/g body weight) [U-^{13}C]-glucose (1g/kg, CLM-1396-PK, Cambridge Isotope Laboratories) in normal saline. 15 or 30 minutes later mice were euthanized, cardiac blood was collected, and tissues were collected and processed. Cardiac puncture blood was added to tubes (Microvette 500Z) on ice, followed by centrifugation according to manufacturer's protocol.

Tissue Processing: Metabolite Extraction: Tissue powder was weighed (~15 mg). For extraction, ice-cold methanol:acetonitrile:water (40:40:20) mixture was added to the powder, vortexed and centrifuged at 16,000 × g for 10 min at 4°C. The volume of the extraction solution (mL) was 40 × the weight of tissue (mg) to make an extract of 25 mg tissue per mL solvent. The supernatant (3 μL) was loaded to LC-MS.

LC-MS: Samples were analyzed using a quadrupole-orbitrap mass spectrometer (Q Exactive Plus, Thermo Fisher Scientific, San Jose, CA) operating in negative or positive ion modes, coupled to hydrophilic interaction chromatography via electrospray ionization and used to scan from m/z 70 to 1000 at 1 Hz and 140,000 resolution. LC separation was on a XBridge BEH Amide column (2.1 mm × 150 mm, 2.5 mm particle size, 130A° pore size) using a gradient of solvent A (20mM ammonium acetate, 20mM ammonium hydroxide in 95:5 water: acetonitrile, pH 9.45) and solvent B (acetonitrile). Flow rate was 150 ml/min. The LC gradient was: 0 min, 85% B; 2 min, 85% B; 3 min, 80% B; 5 min, 80% B; 6 min, 75% B; 7 min, 75% B; 8 min, 70% B; 9 min, 70% B; 10 min, 50% B; 12 min, 50% B; 13 min, 25% B; 16 min, 25% B; 18 min, 0% B; 23 min, 0% B; 24 min, 85% B; 30 min, 85% B. Autosampler temperature was 4°C. Data were analyzed using the MAVEN software[63]. Isotope labeling was corrected for natural 13C abundance using AccuCor[64].

Serum Processing: Method modified from[58]. 2uL of serum was extracted with 80% methanol:water. Samples were centrifuged at 13000xg for 10minutes at 4C. Extracted sample was dried down, methoximated, and derivatized with BSTFA + 1% TMCS. Adonitol

was used as an internal standard. Mass spectral data were obtained on an Agilent 5977B mass-selective detector connected to an 8890 gas chromatograph. The settings are as follows: GC inlet 250 °C, transfer line 280 °C, MS source 230 °C MS Quad 150 °C. An HP-5MS capillary column (30 m length, 250 μm diameter, 0.25 μm film thickness). Agilent MassHunter MS Quantitative Analysis software was used for statistical analysis. ISOCOR was used to normalize data to an internal standard[65].

RNA Sequencing

Sequencing was performed with Novogene, RNA-Seq analyses were performed on the ViaFoundry platform[66]. Briefly, sequence reads were processed with cutadapt (v4.4) to remove adapters and trim low-quality bases. Gene expression was quantified using salmon (v1.9.0) against mouse genome assembly mm10 Gencode m25 basic gene annotation. Differential gene expression analyses were performed using DESeq2 (v1.40.2). Genes failing a minimum read count threshold (10 reads for each replicate in at least one condition) were removed prior to differential expression analysis. Plots were generated using R packages ggplot2 (v.3.4.2), ggrepel (v0.9.3) and pheatmap (v1.0.12) or GraphPadPrism10.

Quantification and Statistical analysis

All data points in the paper are biological replicates, derived from individual mice or cell samples. No statistical methods were used to pre-determine sample sizes, but our sample sizes are similar to those reported in previous publications: Glucose tracing (Jung et al., 2021); Acyl CoA measurements (Martinez-Calejman, 2020), D2O labeling (Sanchez-Gurmaches, 2018). Data distribution was assumed to be normal, but this was not formally tested. Data are presented as mean ±SEM, *$p < 0.05$, **$p < 0.01$, ***$p < 0.001$ and ****$p < 0.0001$ unless stated otherwise. Student's t test or two-way ANOVA with the Tukey's multiple comparisons test, as appropriate, was used to determine statistical significance. Statistical analysis was done using GraphPad Prism 9 and 10.

Extended Data

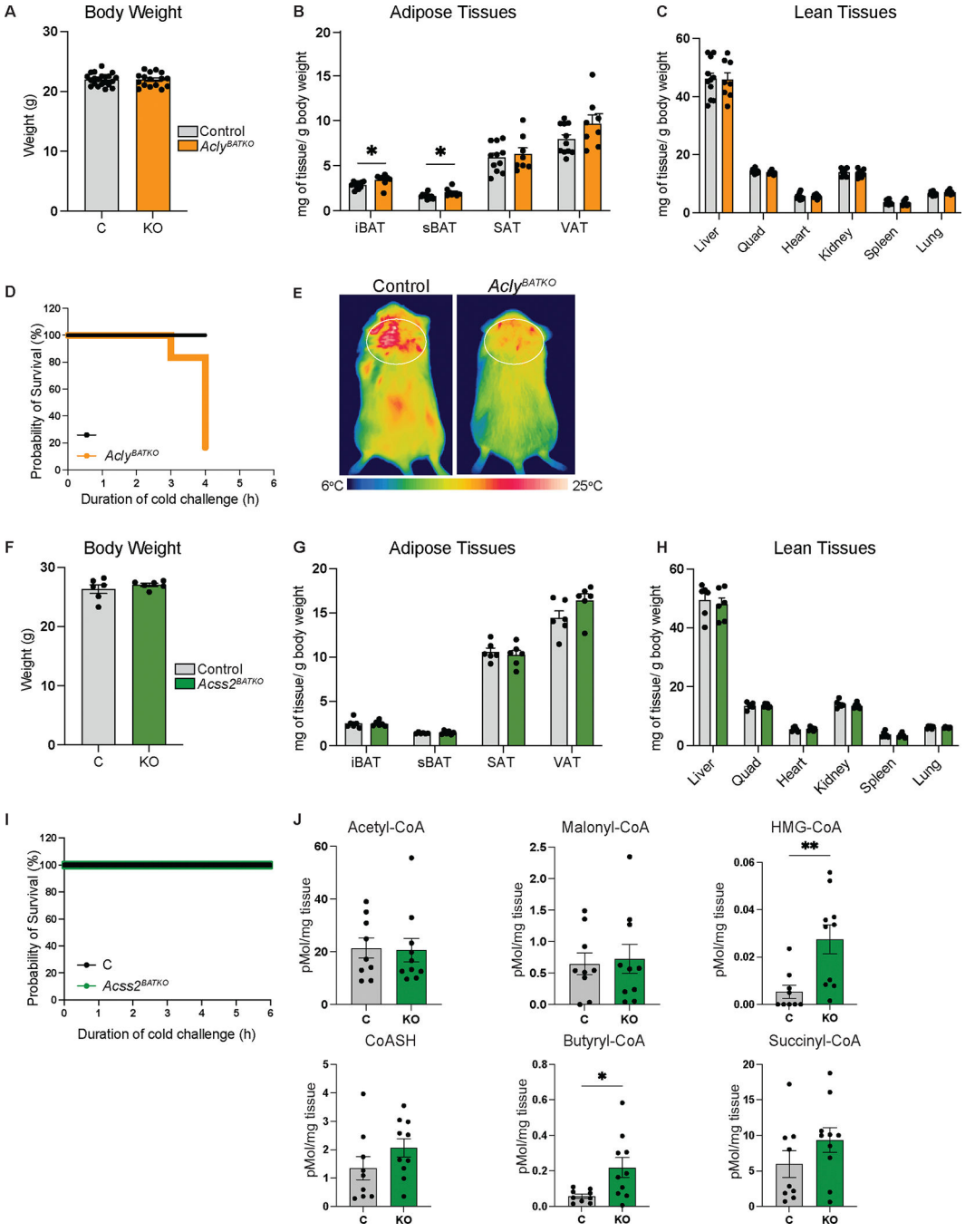

Ext.Data Fig. 1. ACLY loss in Brown Fat Causes Tissue Whitening and Cold Intolerance in Male Mice.

A. Body weight of the *Acly*^{BATKO} male mice. n=21 C, 16 KO.

B. Adipose tissue weights of the *Acly*^{BATKO} male mice. *p= 0.0246, *p= 0.0234. n=11 C, 8 KO.

C. Lean tissue weights of the *Acly*^{BATKO} male mice. n=11 C, 8 KO.

D. “Survival curve” for cold exposure experiment, where mice maintain body temperature above 30°C, remain in the cold over the time course of experiment. n=C, 6 KO.
E. Dorsal view representative infrared thermography image of heat signature of the iBAT from *Acly*^{BATKO} mouse and littermate control.
F. Body weights of the *Acss2*^{BATKO} male mice. n=6 C, 6 KO.
G. Adipose tissue weights of the *Acss2*^{BATKO} male mice. n=6 C, 6 KO.
H. Lean tissue weights of the *Acss2*^{BATKO} male mice. n=6 C, 6 KO.
I. “Survival curve”, how many mice remain in the cold over the time course of experiment. n=6 C, 6 KO.
J. Acyl CoA levels measurements in the *Acss2*^{BATKO} male mice BAT. **p= 0.0052, *p= 0.0170. n=9 C, 10 KO.
Data are mean ± s.e.m. Statistical analysis unpaired two-tailed Student’s t-test.

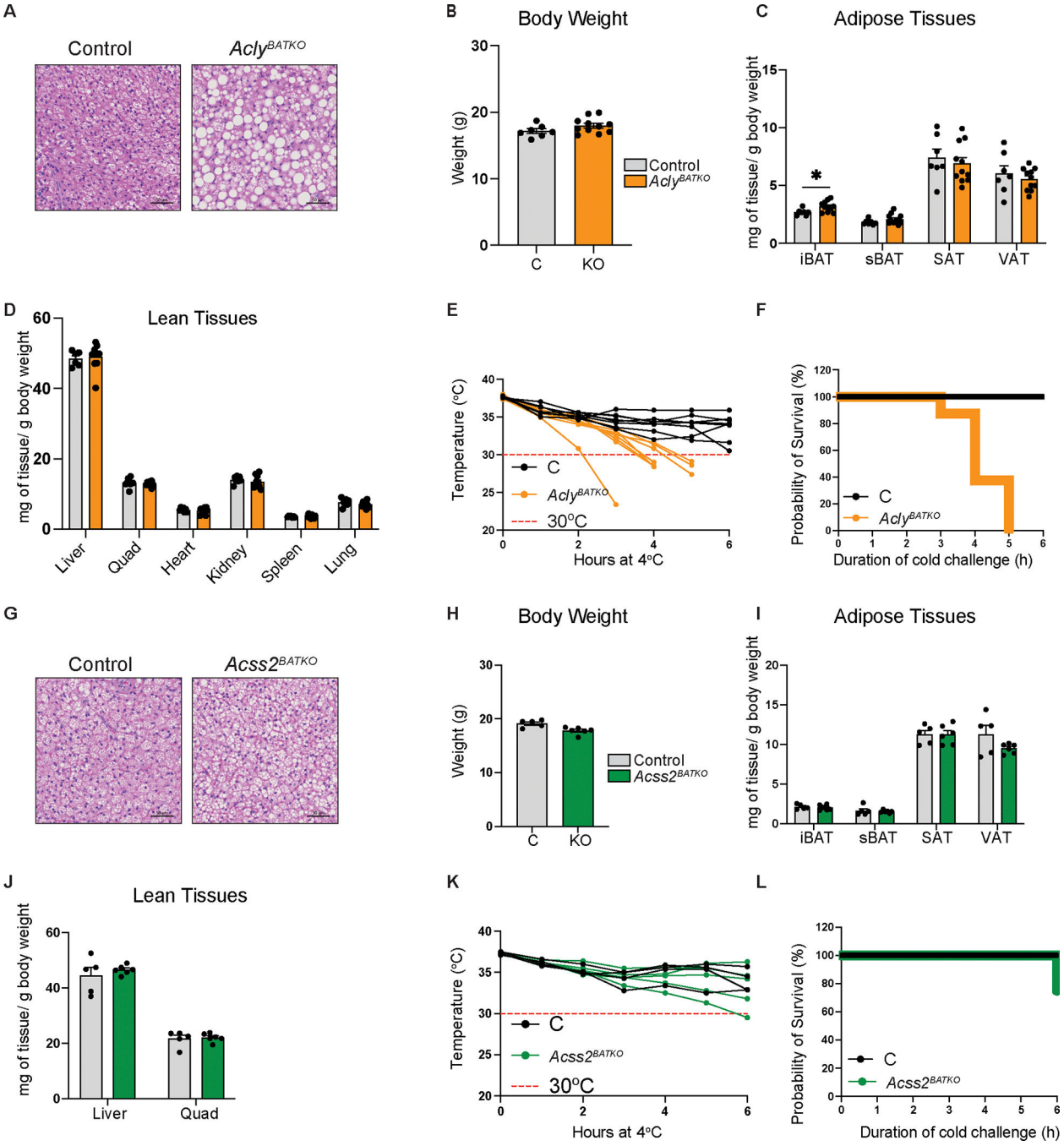

Extended Fig. 2. ACLY loss in Brown Fat Causes Tissue Whitening and Cold Intolerance in Female Mice.

A. Representative H&E of the iBAT from *Acly*^{BATKO} female mouse and littermate control. Scale bar 50um. Clear consistent phenotype across n=3 mice.

B. Body weight of the *Acly*^{BATKO} female mice. n=7 C, 11 KO.

C. Adipose tissue weights of the *Acly*^{BATKO} female mice. *p= 0.0232. n=7 C, 11 KO.

D. Lean tissue weights of the *Acly*^{BATKO} female mice. n=7 C, 11 KO.

E. Rectal temperatures of the *Acly*^{BATKO} female mice and littermate controls during cold exposure (4°C). n=8 C, 8 KO.

F. “Survival curve”, how many mice maintain body temperature above 30°C, remain in the cold over the time course of experiment. n=8 C, 8 KO.
G. Representative H&E of the iBAT from *Acss2*^{BATKO} female mouse and littermate control. Scale bar 50um. Consistent across n=6 mice.
H. Body weight of the *Acss2*^{BATKO} female mice. n=5 C, 6 KO.
I. Adipose tissue weights of the *Acss2*^{BATKO} female mice. n=5 C, 6 KO.
J. Lean tissue weights of the *Acss2*^{BATKO} female mice. n=5 C, 6 KO.
K. Rectal temperatures of the *Acss2*^{BATKO} female mice and littermate controls during cold exposure (4°C). n=4 C, 5 KO.
L. “Survival curve”, how many mice maintain body temperature above 30°C, remain in the cold over the time course of experiment. n=4 C, 5 KO.
Data are mean ± s.e.m. Statistical analysis unpaired two-tailed Student’s t-test.

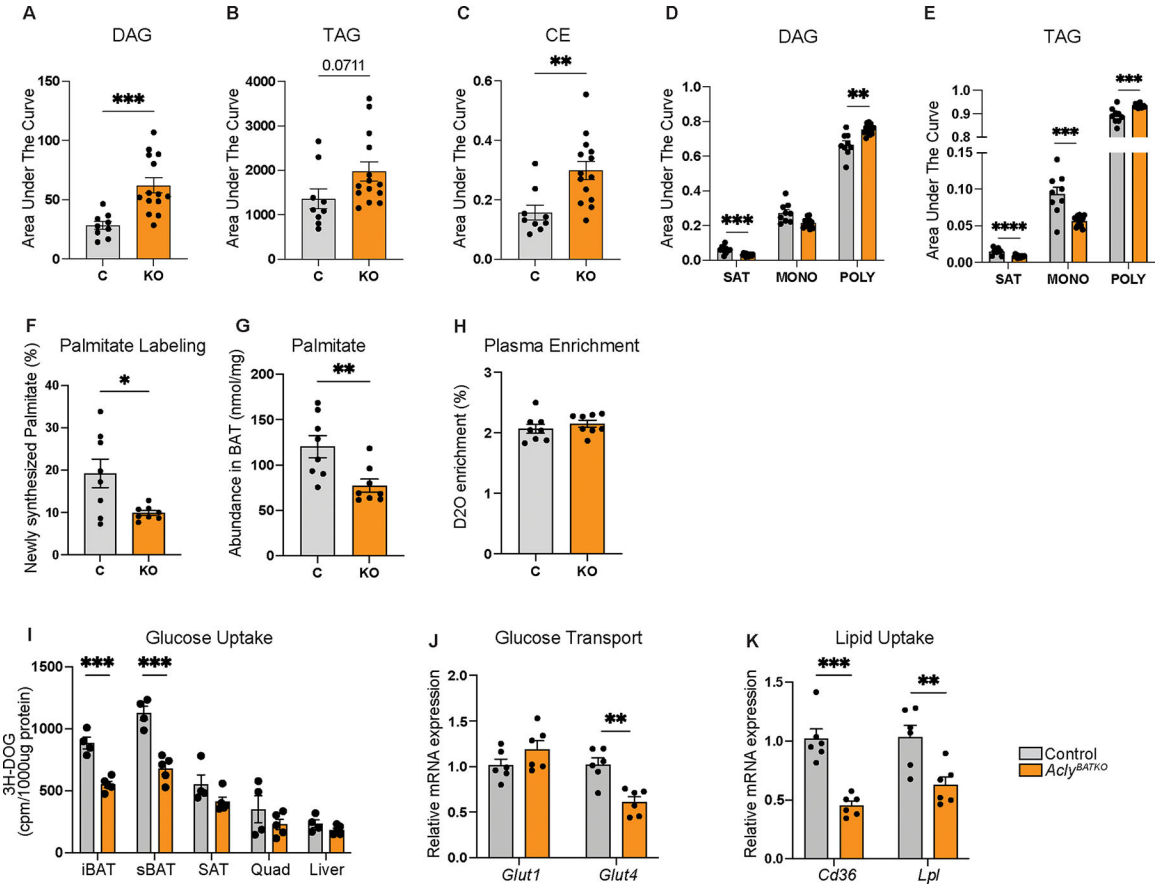

Extended Fig. 3. BAT ACLY Loss Broadly Impairs Metabolism.
A. Lipidomics analysis of DAG in the *Acly*^{BATKO} mice BAT. ***p= 0.0007. n=9 C, 14 KO.
B. Lipidomics analysis of TAG in the *Acly*^{BATKO} mice BAT. n=9 C, 14 KO.
C. Lipidomics analysis of CE in the *Acly*^{BATKO} mice BAT. **p= 0.0035. n=9 C, 14 KO.
D. Lipidomics analysis of DAG degree of saturation in the *Acly*^{BATKO} mice BAT. ***p= 0.0001, **p= 0.0002. n=9 C, 14 KO.
E. Lipidomics analysis of TAG degree of saturation in the *Acly*^{BATKO} mice BAT. **** <0.0001, ***p= 0.0001, ***p= 0.0002. n=9 C, 14 KO.

F. D2O labeling of newly synthesized palmitate in the $Acly^{BATKO}$ mice BAT and their littermates. *p= 0.0163. n=8 C, 8 KO.
G. Palmitate abundance in BAT of $Acly^{BATKO}$ mice and littermate controls. **p= 0.0087. n=8 C, 8 KO.
H. D2O enrichment in plasma of $Acly^{BATKO}$ mice and littermate controls. n=8 C, 8 KO.
I. 3H-2-deoxy-glucose uptake assay into interscapular BAT, subscapular BAT, SAT, Quad and Liver of the $Acly^{BATKO}$ mice after 30 min at 4°C. ***p= 0.0003, ***p= 0.0004. n=4 C, 5 KO.
J. RT-PCR analysis of *Glut1* and *Glut4* in the $Acly^{BATKO}$ mice BAT. **p= 0.0015. n=6 C, 6 KO.
K. RT-PCR analysis of *cd36* and *lpl* in the $Acly^{BATKO}$ mice BAT. ***p= 0.0001, **p= 0.0072. n=6 C, 6 KO.
Panels A-K: grey bar (C), orange bar ($Acly^{BATKO}$).
Data are mean ± s.e.m. Statistical analysis unpaired two-tailed Student's t-test.

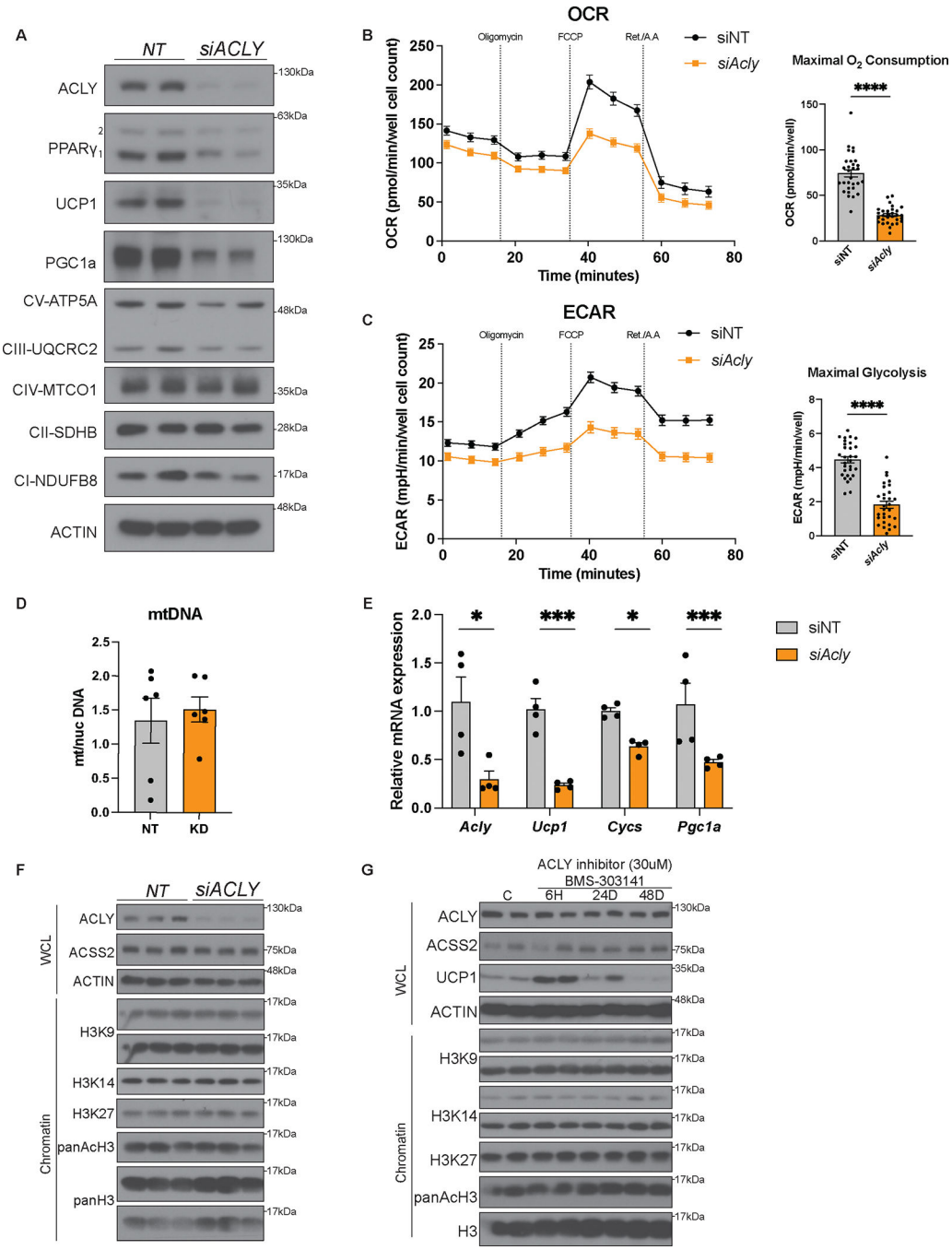

Extended Fig. 4. The Thermogenic Gene Program Requires ACLY.

A. Western blot of siACLY treated brown mature adipocytes. n=2 samples, result has been replicated.

B. Seahorse Mito Stress Test OCR measurements of siACLY treated brown mature adipocytes. ****p <0.0001. n=30NT, n=30 siACLY wells, result has been replicated.

C. Seahorse Mito Stress Test ECAR measurements of siACLY treated brown mature adipocytes. ****p <0.0001. n=30NT, n=30 siACLY wells, result has been replicated.

D. Mitochondria/Nuclear DNA ratio in the siACLY treated brown mature adipocytes. n=6 C, 6 KO.

E. RT-PCR analysis of *Acly, Ucp1, Cycs and Pgc1a* in the siRNA treated brown mature adipocytes.*p=0.0251, ***p= 0.0005, *p=0.0004, ***p=0.0373. n=4 C, 4 KO.

F. Western blot of siACLY treated brown mature adipocytes, chromatin and WCL (whole cell lysate). n=3 samples.

G. Western blot of ACLY inhibitor (BMS-303141) treated brown mature adipocytes, chromatin and WCL (whole cell lysate). n=2 samples.

Panels B-E: grey bar (NT), orange bar (si*Acly).*

Panels B, C: black line (NT), orange line (si*Acly).*

Data are mean ± s.e.m. Statistical analysis unpaired two-tailed Student's t-test.

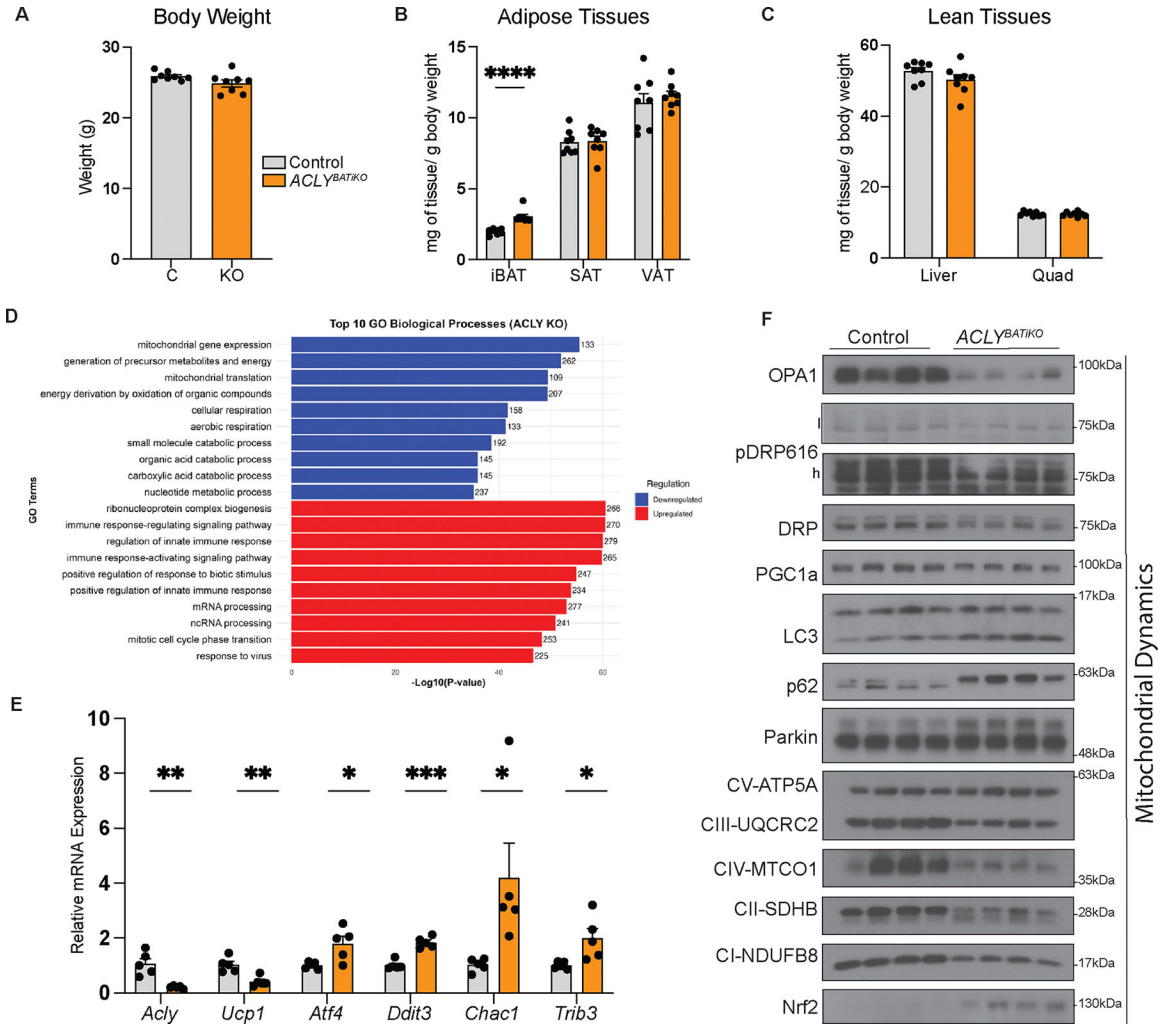

Extended Fig. 5. Induced ACLY loss triggers the Integrated Stress Response and Changes in Mitochondrial Processes.

A. Body weight of the AclyBATiKO male mice. n=8 C, 8 KO.

B. Adipose tissue weights of the AclyBATiKO male mice. ****p=<0.0001. n=8 C, 8 KO.

C. Lean tissue weights of the AclyBATiKO male mice. n=8 C, 8 KO.

D. RT-PCR analysis of iBAT from AclyBATiKO male mice and littermate controls. **p=0.0020, **p=0.0031, *p=0.0205, ***p<0.0001, *p=0.0380, *p=0.0254 n=5 C, 5 KO.
F. Western blot of the AclyBATiKO male mice. N=4 individual mice.
Panels A-D: grey bar (C), orange bar (AclyBATiKO).
Data are mean ± s.e.m. Statistical analysis unpaired two-tailed Student's t-test.

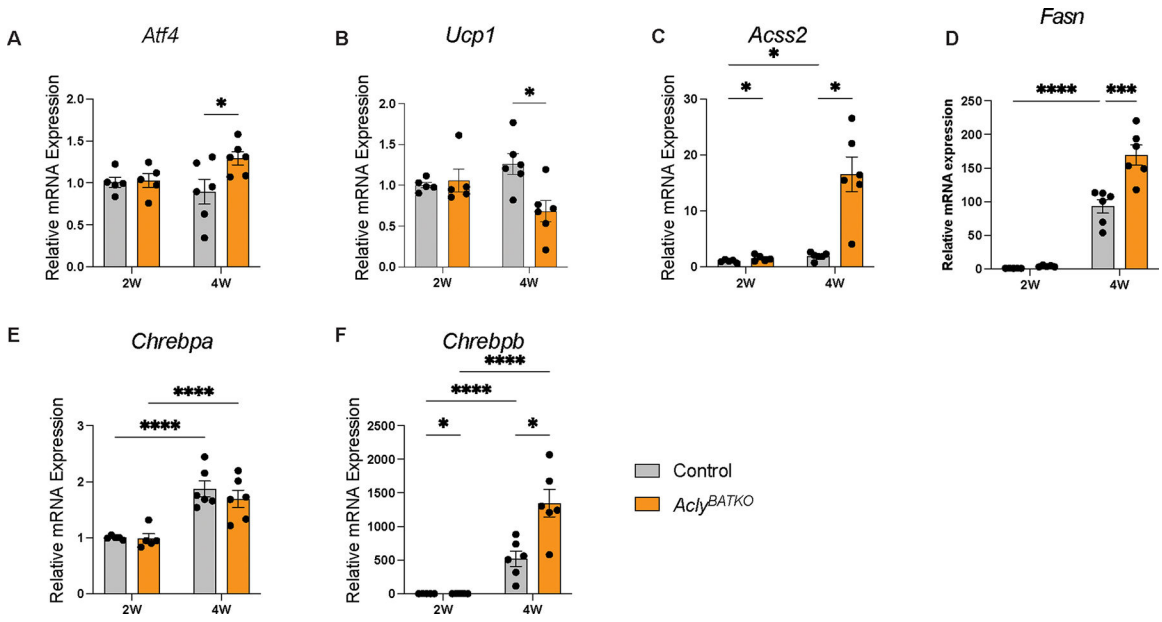

Extended Fig. 6. ACLY's Role in Mitigating Stress is Linked to Dietary Carbohydrates.
A. RT-PCR analysis of *Atf4* in the *Acly*^{BATKO} mice 2 and 4 week of age. *p=0.0496. 2W: n=5 C, 5 KO; 4W: n=6 C, 6 KO.
B. RT-PCR analysis of *Ucp1* in the *Acly*^{BATKO} mice 2 and 4 week of age. *p=0.0106.
C. RT-PCR analysis of *Acss2* in the *Acly*^{BATKO} mice 2 and 4 week of age. *p=0.0110, p*=0.0110, *p=0.0145.
D. RT-PCR analysis of *Fasn* in the *Acly*^{BATKO} mice 2 and 4 week of age.****p<0.0001, ***p=0.0001.
E. RT-PCR analysis of *Chrebpa* in the *Acly*^{BATKO} mice 2 and 4 week of age. ****p<0.0001, ****p<0.0001.
F. RT-PCR analysis of *Chrebpb* in the *Acly*^{BATKO} mice 2 and 4 week of age. *p=0.0434, *p=0.0434, ****p<0.0001, ****p<0.0001.
Panels A-F: grey bar (C), orange bar (*Acly*^{BATKO}).
Data are mean ± s.e.m. Group differences determined via one-tailed ANOVA with Tukey's post hoc.

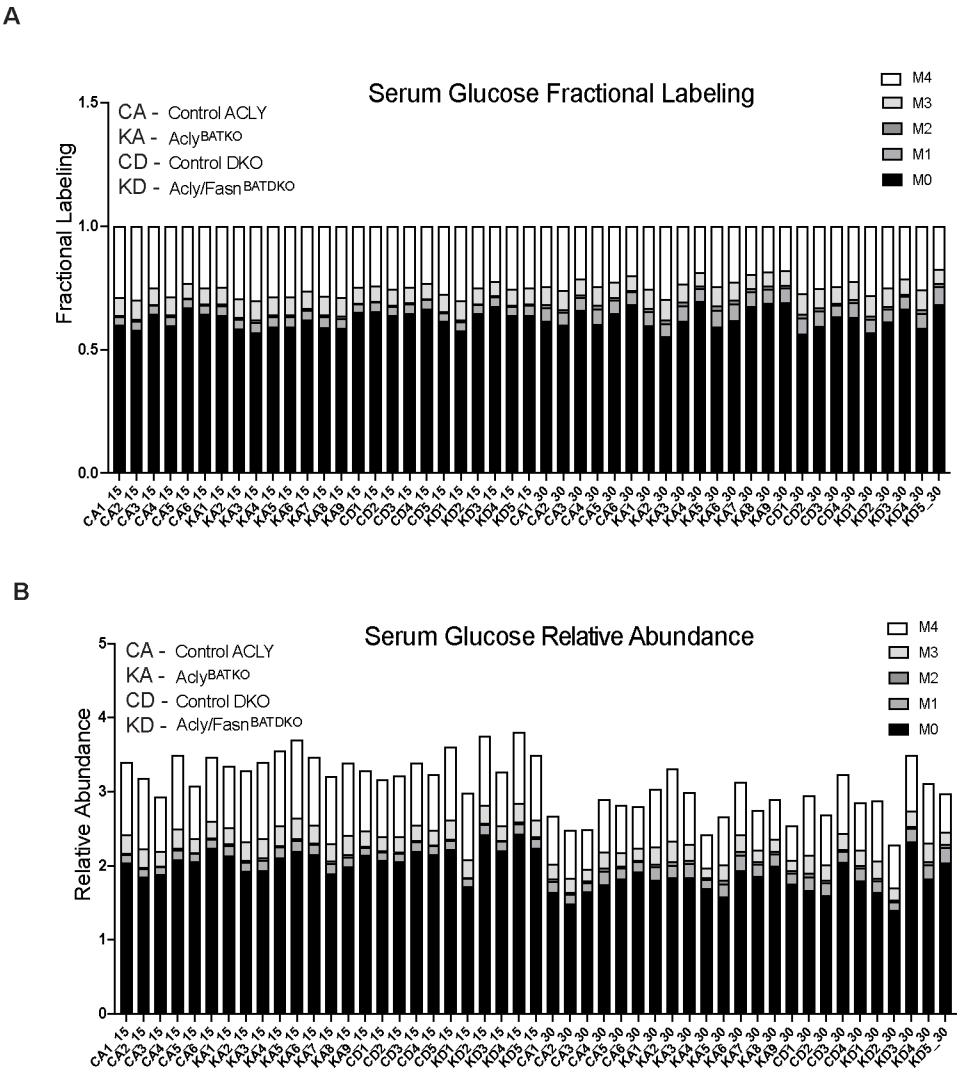

Extended Fig. 7. ACLY Prevents TCA Cycle Overload During Thermogenesis.

A. Serum glucose fractional labeling *Acly*^{BATKO} and *Acly,Fasn*^{BATKO} mice.

B. Serum glucose relative abundance *Acly*^{BATKO} and *Acly,Fasn*^{BATKO} mice.

15 minutes: *Acly*^{BATKO} n=6C, 9 KO; *Acly,Fasn*^{BATKO} n=5C, 5 KO. 30 minutes: *Acly*^{BATKO} n=6C, 9 KO; *Acly,Fasn*^{BATKO} n=4, 5 KO.

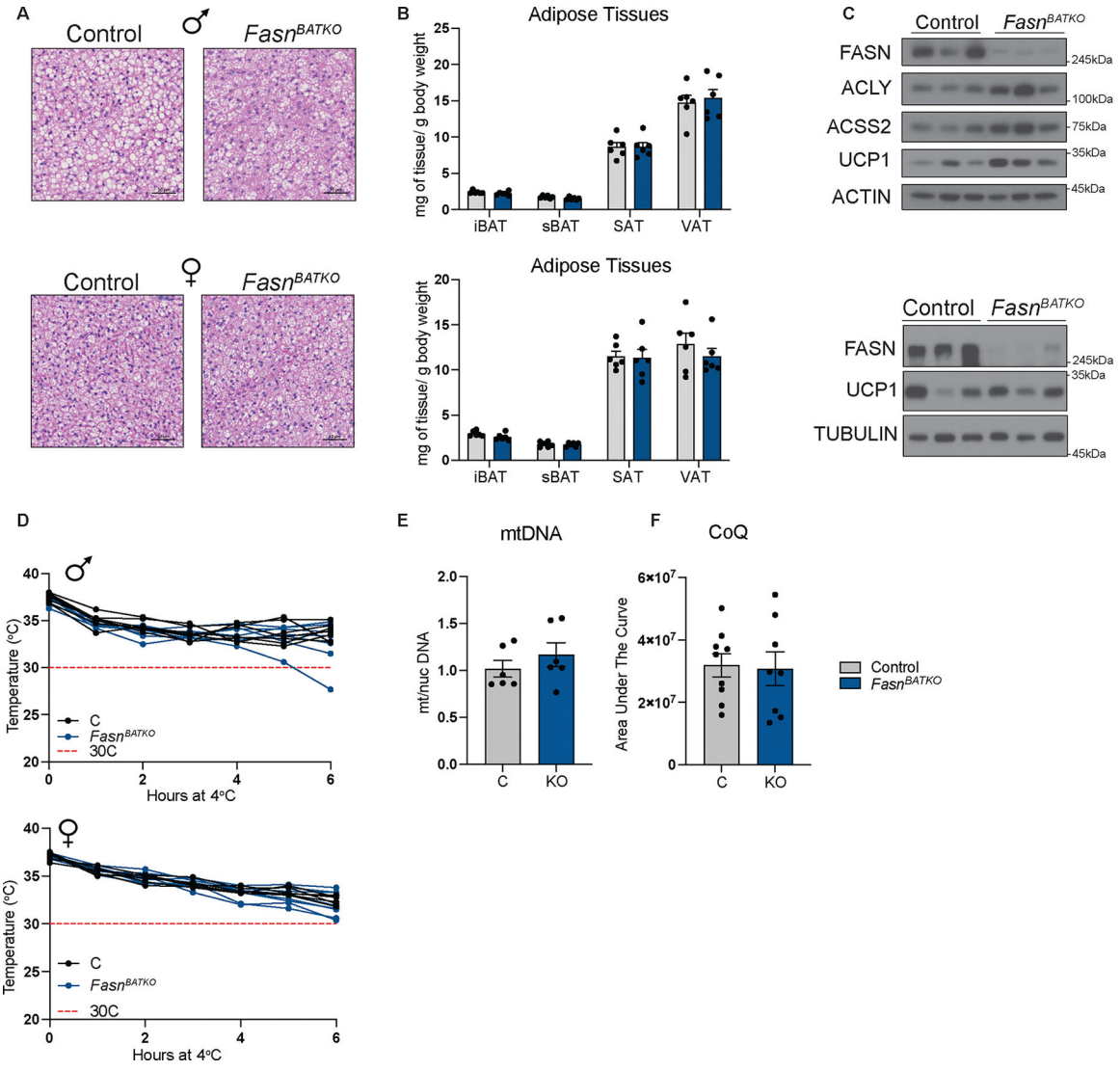

Extended Fig. 8. *Fasn*^{BATKO} male and female mice.

A. Representative H&E of the iBAT from *Fasn*^{BATKO} male and female mouse and littermate control. Scale bar 50um. Has been confirmed in n=3 males, n=5 females.

B. Adipose tissue weights of the *Fasn*^{BATKO} male mice. n=6 C, 6 KO. Adipose tissue weights of the *Fasn*^{BATKO} female mice. n=6 C, 6 KO.

C. Western blot of the *Fasn*^{BATKO} male and female mice.

D. Rectal temperatures of the *Fasn*^{BATKO} male mice and littermate controls during cold exposure (4°C). n=7 C, 7 KO. Rectal temperatures of the *Fasn*^{BATKO} female mice and littermate controls during cold exposure (4°C). n=8 C, 6 KO.

E. Mitochondria/Nuclear DNA ratio in the *Fasn*^{BATKO} mice BAT. n=6 C, 6 KO.

F. CoQ levels in the *Fasn*^{BATKO} mice BAT. n=9 C, 8 KO.

Panels B, E, F: grey bars (C), blue bars (*Fasn*^{BATKO}).

Panel D: black lines (C), blue lines (*Fasn*^{BATKO}).

Data are mean ± s.e.m. Statistical analysis unpaired two-tailed Student's t-test.

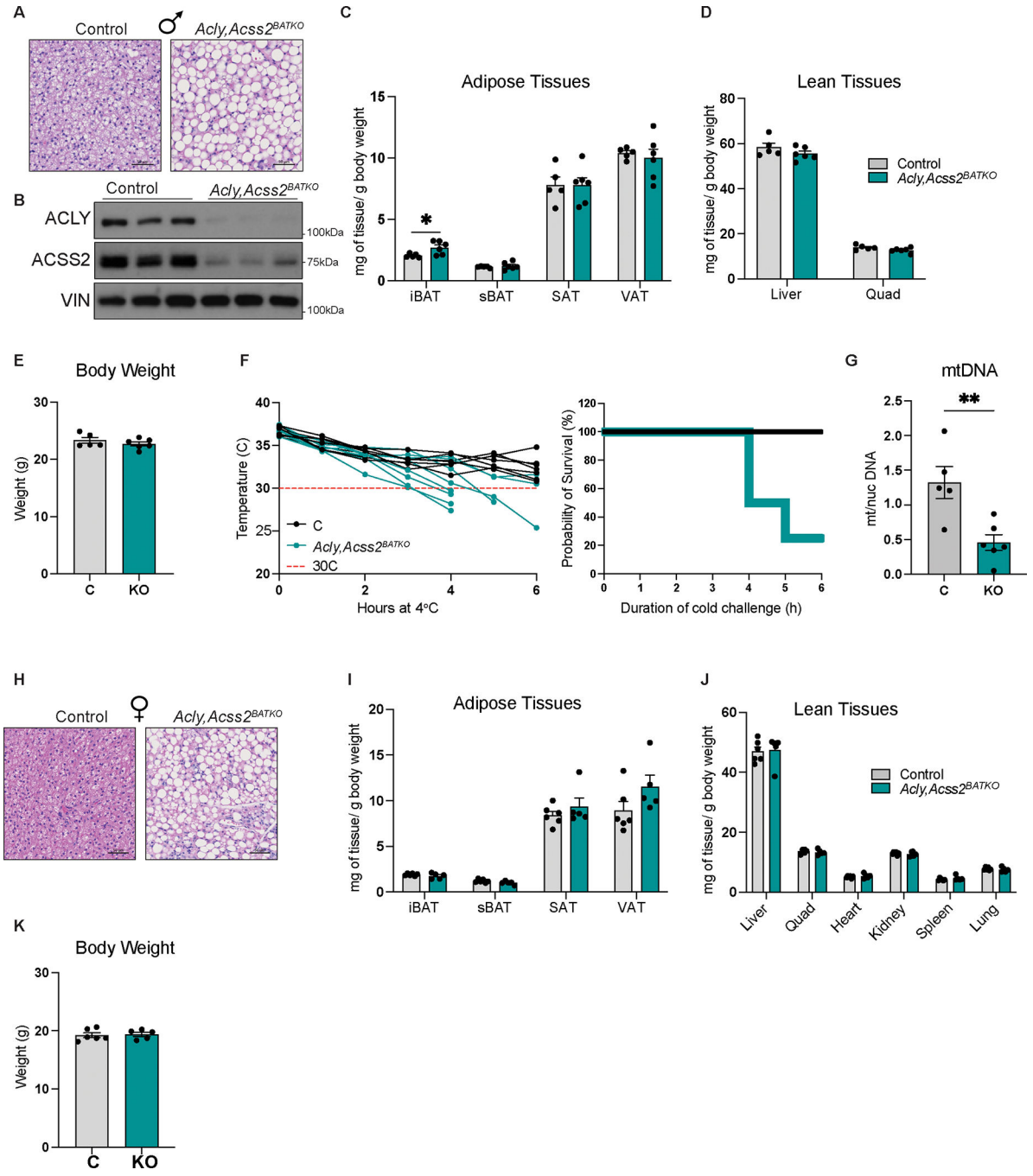

Extended Fig. 9. *Acly,Acss2*^{BATDKO} male and female mice.

A. Representative H&E of the iBAT from *Acly,Acss2*^{BATKO} male mouse and littermate control. Scale bar 50um. Clear consistent phenotype, confirmed n=6 mice.

B. Western blot of the *Acly,Acss2*^{BATKO} male mouse BAT.

C. Adipose tissue weights of the *Acly,Acss2*^{BATKO} male mice. *p=0.0291. n=5 C, 6 KO.

D. Lean tissue weights of the *Acly,Acss2*^{BATKO} male mice. n=5 C, 6 KO.

E. Body weight of the *Acly,Acss2*^{BATKO} male mice. n=5 C, 6 KO.

F. Rectal temperatures of the *Acly,Acss2*^{BATKO} male mice and littermate controls during cold exposure (4°C), left. “Survival curve”, how many mice remain in the cold over the time course of experiment, right. n=7 C, 8 KO.
G. Mitochondria/Nuclear DNA ratio in the *Acly,Acss2BATKO* male mice BAT. **p=0.0060. n=5 C, 6 KO.
H. Representative H&E of the iBAT from *Acly,Acss2*^{BATKO} female mouse and littermate control. Scale bar 50um. Clear consistent phenotype, confirmed in n=4 mice.
I. Adipose tissue weights of the *Acly,Acss2*^{BATKO} female mice. n=6 C, 5 KO.
J. Lean tissue weights of the *Acly,Acss2*^{BATKO} female mice. n=6 C, 5 KO.
K. Body weight of the *Acly, Acss2*^{BATKO} female mice. n=6 C, 5 KO.
Panels C-E,G: grey bars (C), teal (*Acly,Acss2*^{BATKO}) males.
Panels I-K: grey bars (C), blue bars (*Acly,Acss2*^{BATKO}) females.
Panels F: black lines (C), teal lines (*Acly,Acss2*^{BATKO}).
Data are mean ± s.e.m. Statistical analysis unpaired two-tailed Student’s t-test.

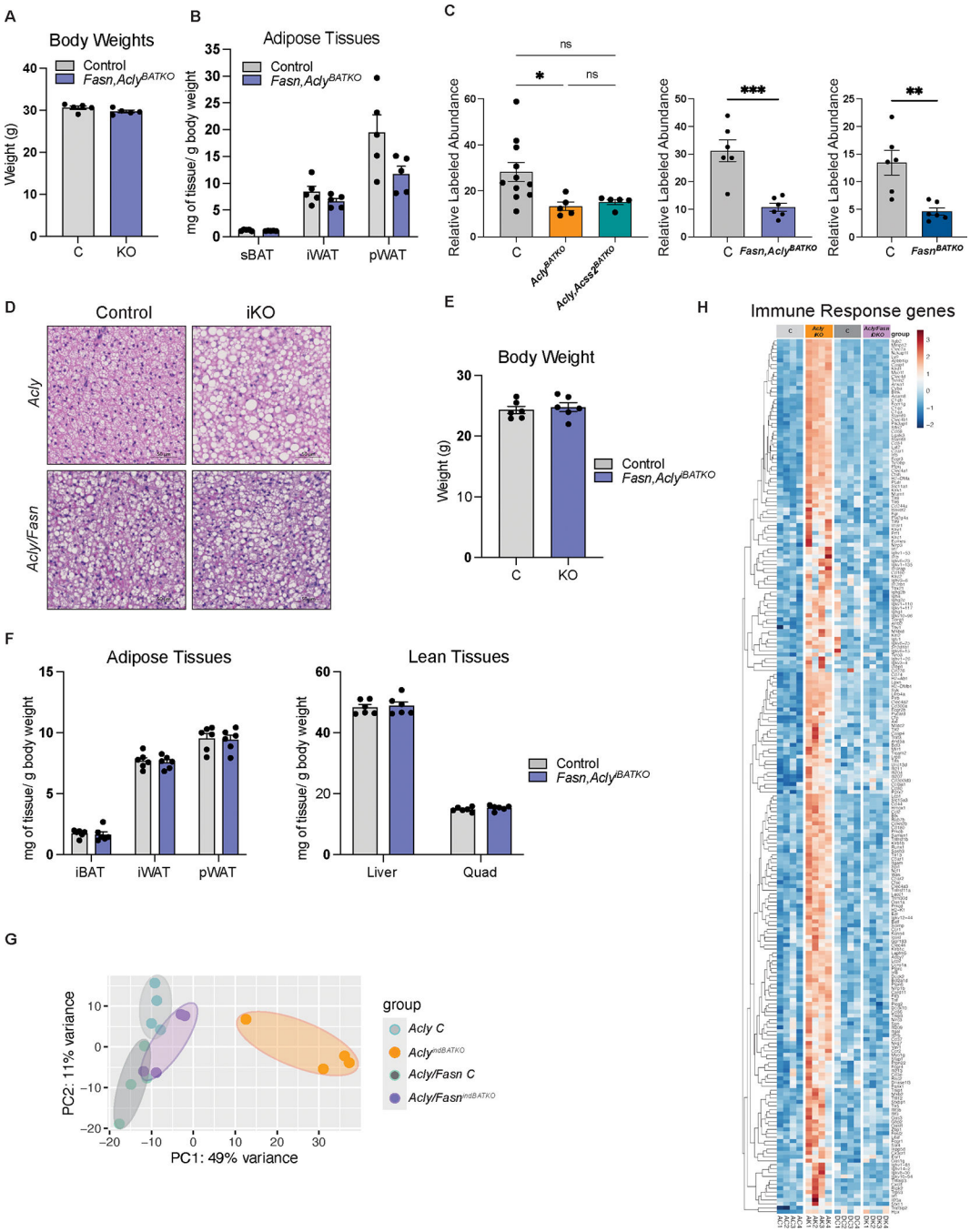

Extended Fig. 10. BAT *Acly;Fasn* Double Knockout Rescues Thermogenesis Independent of DNL and Prevents ISR.

A. Body weight of the *Acly,Fasn*^{BATKO} male mice. n=5 C, 5 KO.

B. Adipose tissue weights of the *Acly,Fasn*^{BATKO} male mice. n=5 C, 5 KO.

C. Relative labeled abundance of palmitate in BAT of Acly^{BATKO},Acss2^{BATKO}(n=11C, 5KO and 5KO), Fasn^{BATKO}(n=6C, 6KO),Acly/Fasn^{BATKO}(n=6C, 6KO)mice and littermate controls. *p=0.0404, ***p= 0.0007, **p=0.0035.

D. Representative H&E of the iBAT from *Acly*^{BATiKO} and *Acly,Fasn*^{BATiKO} male mouse and littermate control. Scale bar 50um. Has been confirmed in n=3 mice each.

E. Body weight of the *Acly,Fasn*^{BATiKO} male mice. n=6 C, 6 KO.
F. Adipose tissue and lean tissues weights of the *Acly,Fasn*^{BATiKO} male mice. n=6 C, 6 KO.
G. Principal Component Analysis (PCA) plot of RNAseq from *Acly*^{BATiKO} and *Acly,Fasn*^{BATiKO} male mouse and littermate controls.
H. Heat map relative abundance of Immune Response genes in RNAseq of *Acly*^{BATiKO} and *Fasn,Acly*^{BATiKO} BAT.
Panel G-H: light grey (C), orange bar (*Acly*^{BATiKO}), dark grey (C), light purple bar (*Fasn,Acly*^{BATiKO}).
Data are mean ± s.e.m. Statistical analysis unpaired two-tailed Student's t-test. Group differences determined via one-tailed ANOVA with Tukey's post hoc.

Acknowledgments

We would like to thank the UMass Chan Morphology Core, Mouse Facility, EM Facility, and members of the Guertin, Wellen, Snyder and Jang labs for helpful discussions.

Funding

This work was funded by R01DK116005, R01DK127175 and R01DK094004 to D.A.G.

M.D.L. was supported by NIH fellowship K01DK111714.

Data and materials availability

All data are available in the main text or the supplementary materials. RNAseq data is available at the NCBI BioSample Project: PRJNA1151645.

References

1. Cannon B & Nedergaard J Brown adipose tissue: function and physiological significance. Physiol Rev 84, 277–359, doi:10.1152/physrev.00015.2003 (2004). [PubMed: 14715917]
2. Cohen P & Kajimura S The cellular and functional complexity of thermogenic fat. Nat Rev Mol Cell Biol 22, 393–409, doi:10.1038/s41580-021-00350-0 (2021). [PubMed: 33758402]
3. Jung SM, Sanchez-Gurmaches J & Guertin DA Brown Adipose Tissue Development and Metabolism. Handb Exp Pharmacol 251, 3–36, doi:10.1007/164_2018_168 (2019). [PubMed: 30203328]
4. Sanchez-Gurmaches J, Hung CM & Guertin DA Emerging Complexities in Adipocyte Origins and Identity. Trends Cell Biol 26, 313–326, doi:10.1016/j.tcb.2016.01.004 (2016). [PubMed: 26874575]
5. Seki T et al. Brown-fat-mediated tumour suppression by cold-altered global metabolism. Nature 608, 421–428, doi:10.1038/s41586-022-05030-3 (2022). [PubMed: 35922508]
6. Becher T et al. Brown adipose tissue is associated with cardiometabolic health. Nat Med 27, 58–65, doi:10.1038/s41591-020-1126-7 (2021). [PubMed: 33398160]
7. Wolfrum C & Gerhart-Hines Z Fueling the fire of adipose thermogenesis. Science 375, 1229–1231, doi:10.1126/science.abl7108 (2022). [PubMed: 35298244]
8. Villarroya J et al. New insights into the secretory functions of brown adipose tissue. J Endocrinol 243, R19–R27, doi:10.1530/JOE-19-0295 (2019). [PubMed: 31419785]
9. Haley JA, Jang C & Guertin DA A new era of understanding in vivo metabolic flux in thermogenic adipocytes. Curr Opin Genet Dev 83, 102112, doi:10.1016/j.gde.2023.102112 (2023). [PubMed: 37703635]
10. Hankir MK & Klingenspor M Brown adipocyte glucose metabolism: a heated subject. EMBO Rep 19, doi:10.15252/embr.201846404 (2018).

11. McCormack JG & Denton RM Evidence that fatty acid synthesis in the interscapular brown adipose tissue of cold-adapted rats is increased in vivo by insulin by mechanisms involving parallel activation of pyruvate dehydrogenase and acetyl-coenzyme A carboxylase. Biochem J 166, 627–630, doi:10.1042/bj1660627 (1977). [PubMed: 23106]
12. Trayhurn P Fatty acid synthesis in mouse brown adipose tissue. The influence of environmental temperature on the proportion of whole-body fatty acid synthesis in brown adipose tissue and the liver. Biochim Biophys Acta 664, 549–560, doi:10.1016/0005-2760(81)90132-6 (1981). [PubMed: 7272321]
13. Mottillo EP et al. Coupling of lipolysis and de novo lipogenesis in brown, beige, and white adipose tissues during chronic beta3-adrenergic receptor activation. J Lipid Res 55, 2276–2286, doi:10.1194/jlr.M050005 (2014). [PubMed: 25193997]
14. Sanchez-Gurmaches J et al. Brown Fat AKT2 Is a Cold-Induced Kinase that Stimulates ChREBP-Mediated De Novo Lipogenesis to Optimize Fuel Storage and Thermogenesis. Cell Metab 27, 195–209 e196, doi:10.1016/j.cmet.2017.10.008 (2018). [PubMed: 29153407]
15. Jung SM et al. In vivo isotope tracing reveals the versatility of glucose as a brown adipose tissue substrate. Cell Rep 36, 109459, doi:10.1016/j.celrep.2021.109459 (2021). [PubMed: 34320357]
16. Zhang Z et al. Serine catabolism generates liver NADPH and supports hepatic lipogenesis. Nat Metab 3, 1608–1620, doi:10.1038/s42255-021-00487-4 (2021). [PubMed: 34845393]
17. Zhao S et al. ATP-Citrate Lyase Controls a Glucose-to-Acetate Metabolic Switch. Cell Rep 17, 1037–1052, doi:10.1016/j.celrep.2016.09.069 (2016). [PubMed: 27760311]
18. Guertin DA & Wellen KE Acetyl-CoA metabolism in cancer. Nat Rev Cancer 23, 156–172, doi:10.1038/s41568-022-00543-5 (2023). [PubMed: 36658431]
19. Park G et al. Quantitative analysis of metabolic fluxes in brown fat and skeletal muscle during thermogenesis. Nat Metab, doi:10.1038/s42255-023-00825-8 (2023).
20. Trayhurn P Fatty acid synthesis in vivo in brown adipose tissue, liver and white adipose tissue of the cold-acclimated rat. FEBS Lett 104, 13–16, doi:10.1016/0014-5793(79)81075-3 (1979). [PubMed: 477972]
21. Lundgren P et al. A subpopulation of lipogenic brown adipocytes drives thermogenic memory. Nat Metab 5, 1691–1705, doi:10.1038/s42255-023-00893-w (2023). [PubMed: 37783943]
22. de Jong JMA et al. Human brown adipose tissue is phenocopied by classical brown adipose tissue in physiologically humanized mice. Nat Metab 1, 830–843, doi:10.1038/s42255-019-0101-4 (2019). [PubMed: 32694768]
23. Martinez Calejman C et al. mTORC2-AKT signaling to ATP-citrate lyase drives brown adipogenesis and de novo lipogenesis. Nat Commun 11, 575, doi:10.1038/s41467-020-14430-w (2020). [PubMed: 31996678]
24. Fernandez S et al. Adipocyte ACLY Facilitates Dietary Carbohydrate Handling to Maintain Metabolic Homeostasis in Females. Cell Rep 27, 2772–2784 e2776, doi:10.1016/j.celrep.2019.04.112 (2019). [PubMed: 31141698]
25. Seale P Transcriptional Regulatory Circuits Controlling Brown Fat Development and Activation. Diabetes 64, 2369–2375, doi:10.2337/db15-0203 (2015). [PubMed: 26050669]
26. Shapira SN & Seale P Transcriptional Control of Brown and Beige Fat Development and Function. Obesity (Silver Spring) 27, 13–21, doi:10.1002/oby.22334 (2019). [PubMed: 30569639]
27. Angueira AR et al. Early B Cell Factor Activity Controls Developmental and Adaptive Thermogenic Gene Programming in Adipocytes. Cell Rep 30, 2869–2878 e2864, doi:10.1016/j.celrep.2020.02.023 (2020). [PubMed: 32130892]
28. Han S et al. Mitochondrial integrated stress response controls lung epithelial cell fate. Nature 620, 890–897, doi:10.1038/s41586-023-06423-8 (2023). [PubMed: 37558881]
29. Yuliana A et al. Endoplasmic Reticulum Stress Impaired Uncoupling Protein 1 Expression via the Suppression of Peroxisome Proliferator-Activated Receptor γ Binding Activity in Mice Beige Adipocytes. International Journal of Molecular Sciences 20, doi:10.3390/ijms20020274 (2019).
30. Sustarsic EG et al. Cardiolipin Synthesis in Brown and Beige Fat Mitochondria Is Essential for Systemic Energy Homeostasis. Cell Metabolism 28, 159–174.e111, doi:10.1016/j.cmet.2018.05.003 (2018). [PubMed: 29861389]

31. Costa-Mattioli M & Walter P The integrated stress response: From mechanism to disease. Science 368, doi:10.1126/science.aat5314 (2020).
32. Souza-Mello V, Bond LM, Burhans MS & Ntambi JM Uncoupling protein-1 deficiency promotes brown adipose tissue inflammation and ER stress. Plos One 13, doi:10.1371/journal.pone.0205726 (2018).
33. Lu Y et al. Mitophagy is required for brown adipose tissue mitochondrial homeostasis during cold challenge. Sci Rep 8, 8251, doi:10.1038/s41598-018-26394-5 (2018). [PubMed: 29844467]
34. Wikstrom JD et al. Hormone-induced mitochondrial fission is utilized by brown adipocytes as an amplification pathway for energy expenditure. EMBO J 33, 418–436, doi:10.1002/embj.201385014 (2014). [PubMed: 24431221]
35. Rahbani JF et al. Creatine kinase B controls futile creatine cycling in thermogenic fat. Nature 590, 480–485, doi:10.1038/s41586-021-03221-y (2021). [PubMed: 33597756]
36. Mick E et al. Distinct mitochondrial defects trigger the integrated stress response depending on the metabolic state of the cell. Elife 9, doi:10.7554/eLife.49178 (2020).
37. Guilherme A et al. Neuronal modulation of brown adipose activity through perturbation of white adipocyte lipogenesis. Mol Metab 16, 116–125, doi:10.1016/j.molmet.2018.06.014 (2018). [PubMed: 30005879]
38. Romanelli SM et al. BAd-CRISPR: Inducible gene knockout in interscapular brown adipose tissue of adult mice. J Biol Chem 297, 101402, doi:10.1016/j.jbc.2021.101402 (2021). [PubMed: 34774798]
39. Holman CD et al. Aging impairs cold-induced beige adipogenesis and adipocyte metabolic reprogramming. bioRxiv, 2023.2003.2020.533514, doi:10.1101/2023.03.20.533514 (2023).
40. Guilherme A et al. Acetyl-CoA carboxylase 1 is a suppressor of the adipocyte thermogenic program. Cell Rep 42, 112488, doi:10.1016/j.celrep.2023.112488 (2023). [PubMed: 37163372]
41. Quek LE et al. Dynamic (13)C Flux Analysis Captures the Reorganization of Adipocyte Glucose Metabolism in Response to Insulin. iScience 23, 100855, doi:10.1016/j.isci.2020.100855 (2020). [PubMed: 32058966]
42. Jung SM et al. Non-canonical mTORC2 Signaling Regulates Brown Adipocyte Lipid Catabolism through SIRT6-FoxO1. Mol Cell 75, 807–822 e808, doi:10.1016/j.molcel.2019.07.023 (2019). [PubMed: 31442424]
43. Kazak L et al. UCP1 deficiency causes brown fat respiratory chain depletion and sensitizes mitochondria to calcium overload-induced dysfunction. Proc Natl Acad Sci U S A 114, 7981–7986, doi:10.1073/pnas.1705406114 (2017). [PubMed: 28630339]
44. Chang CF et al. Brown adipose tissue CoQ deficiency activates the integrated stress response and FGF21-dependent mitohormesis. EMBO J 43, 168–195, doi:10.1038/s44318-023-00008-x (2024). [PubMed: 38212382]
45. Kim W et al. Polyunsaturated Fatty Acid Desaturation Is a Mechanism for Glycolytic NAD(+) Recycling. Cell Metab 29, 856–870 e857, doi:10.1016/j.cmet.2018.12.023 (2019). [PubMed: 30686744]
46. Sharma AK, Khandelwal R & Wolfrum C Futile cycles: Emerging utility from apparent futility. Cell Metab 36, 1184–1203, doi:10.1016/j.cmet.2024.03.008 (2024). [PubMed: 38565147]
47. Kazak L Promoting metabolic inefficiency for metabolic disease. iScience 26, 107843, doi:10.1016/j.isci.2023.107843 (2023). [PubMed: 37736043]
48. Brownstein AJ, Veliova M, Acin-Perez R, Liesa M & Shirihai OS ATP-consuming futile cycles as energy dissipating mechanisms to counteract obesity. Rev Endocr Metab Disord 23, 121–131, doi:10.1007/s11154-021-09690-w (2022). [PubMed: 34741717]
49. Chen KY et al. Opportunities and challenges in the therapeutic activation of human energy expenditure and thermogenesis to manage obesity. J Biol Chem 295, 1926–1942, doi:10.1074/jbc.REV119.007363 (2020). [PubMed: 31914415]
50. Carpentier AC, Blondin DP, Haman F & Richard D Brown Adipose Tissue-A Translational Perspective. Endocr Rev 44, 143–192, doi:10.1210/endrev/bnac015 (2023). [PubMed: 35640259]
51. Yu SY, Luan Y, Dong R, Abazarikia A & Kim SY Adipose Tissue Wasting as a Determinant of Pancreatic Cancer-Related Cachexia. Cancers (Basel) 14, doi:10.3390/cancers14194754 (2022).

52. Weber BZC, Arabaci DH & Kir S Metabolic Reprogramming in Adipose Tissue During Cancer Cachexia. Front Oncol 12, 848394, doi:10.3389/fonc.2022.848394 (2022). [PubMed: 35646636]
53. Fasshauer M et al. Essential role of insulin receptor substrate 1 in differentiation of brown adipocytes. Mol Cell Biol 21, 319–329, doi:10.1128/MCB.21.1.319-329.2001 (2001). [PubMed: 11113206]
54. Hung CM et al. Rictor/mTORC2 loss in the Myf5 lineage reprograms brown fat metabolism and protects mice against obesity and metabolic disease. Cell Rep 8, 256–271, doi:10.1016/j.celrep.2014.06.007 (2014). [PubMed: 25001283]
55. Quiros PM, Goyal A, Jha P & Auwerx J Analysis of mtDNA/nDNA Ratio in Mice. Curr Protoc Mouse Biol 7, 47–54, doi:10.1002/cpmo.21 (2017). [PubMed: 28252199]
56. Livak KJ & Schmittgen TD Analysis of relative gene expression data using real-time quantitative PCR and the 2(-Delta Delta C(T)) Method. Methods 25, 402–408, doi:10.1006/meth.2001.1262 (2001). [PubMed: 11846609]
57. Wallace M et al. Enzyme promiscuity drives branched-chain fatty acid synthesis in adipose tissues. Nat Chem Biol 14, 1021–1031, doi:10.1038/s41589-018-0132-2 (2018). [PubMed: 30327559]
58. Haley JA et al. Decoupling of Nrf2 Expression Promotes Mesenchymal State Maintenance in Non-Small Cell Lung Cancer. Cancers (Basel) 11, doi:10.3390/cancers11101488 (2019).
59. Simons B et al. Shotgun Lipidomics by Sequential Precursor Ion Fragmentation on a Hybrid Quadrupole Time-of-Flight Mass Spectrometer. Metabolites 2, 195–213, doi:10.3390/metabo2010195 (2012). [PubMed: 24957374]
60. Lynes MD et al. Cold-Activated Lipid Dynamics in Adipose Tissue Highlights a Role for Cardiolipin in Thermogenic Metabolism. Cell Rep 24, 781–790, doi:10.1016/j.celrep.2018.06.073 (2018). [PubMed: 30021173]
61. Frey AJ et al. LC-quadrupole/Orbitrap high-resolution mass spectrometry enables stable isotope-resolved simultaneous quantification and (1)(3)C-isotopic labeling of acyl-coenzyme A thioesters. Anal Bioanal Chem 408, 3651–3658, doi:10.1007/s00216-016-9448-5 (2016). [PubMed: 26968563]
62. Snyder NW et al. Production of stable isotope-labeled acyl-coenzyme A thioesters by yeast stable isotope labeling by essential nutrients in cell culture. Anal Biochem 474, 59–65, doi:10.1016/j.ab.2014.12.014 (2015). [PubMed: 25572876]
63. Melamud E, Vastag L & Rabinowitz JD Metabolomic analysis and visualization engine for LC-MS data. Anal Chem 82, 9818–9826, doi:10.1021/ac1021166 (2010). [PubMed: 21049934]
64. Su X, Lu W & Rabinowitz JD Metabolite Spectral Accuracy on Orbitraps. Anal Chem 89, 5940–5948, doi:10.1021/acs.analchem.7b00396 (2017). [PubMed: 28471646]
65. Millard P et al. IsoCor: isotope correction for high-resolution MS labeling experiments. Bioinformatics 35, 4484–4487, doi:10.1093/bioinformatics/btz209 (2019). [PubMed: 30903185]
66. Yukselen O, Turkyilmaz O, Ozturk AR, Garber M & Kucukural A DolphinNext: a distributed data processing platform for high throughput genomics. BMC Genomics 21, 310, doi:10.1186/s12864-020-6714-x (2020). [PubMed: 32306927]

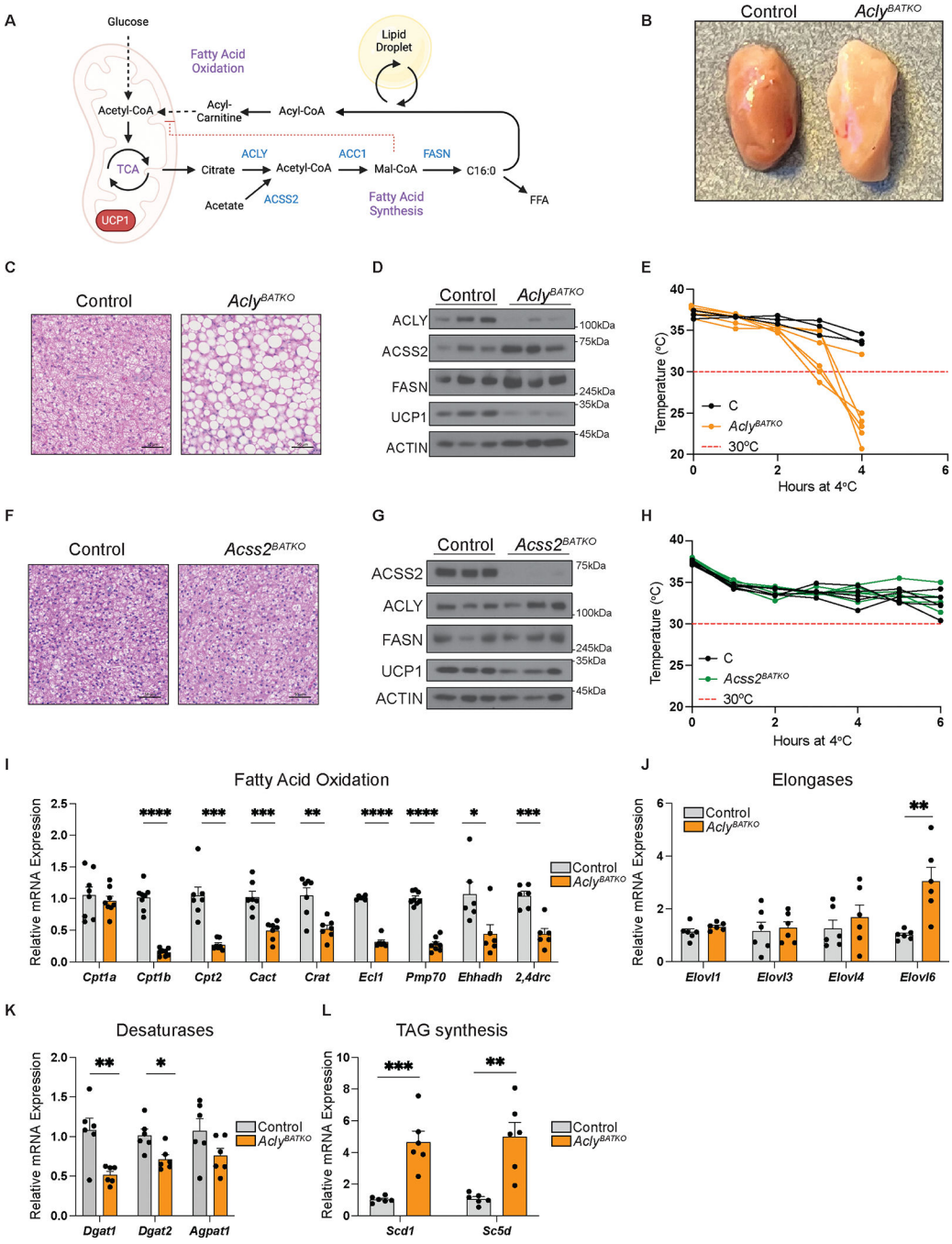

Fig. 1. ACLY loss in Brown Fat Causes Tissue Whitening, Cold Intolerance and Lipid Metabolic Reprogramming in Male Mice.

A. Model of futile FAS-FAO cycling in BAT and the role of ACLY. Created in BioRender. G, D. (2024) BioRender.com/y99u456.

B. Representative image of the interscapular BAT from an *Acly*^{BATKO} mouse and littermate control at 10 weeks old.

C. Representative H&E of the iBAT from *Acly*^{BATKO} male mouse and littermate control. Scale bar 50um. Clear consistent phenotype across n=4 mice.

D. Western blot corresponding to the images in (B) and (C). n=3 mice.

E. Rectal temperatures of the *Acly*^{BATKO} male mice and littermate controls during cold exposure (4°C). n=3 C, 6 KO.

F. Representative H&E of the iBAT from *Acss2*^{BATKO} male mouse and littermate control. Scale bar 50um. Consistent phenotype across n=3 mice.

G. Western blot of the *Acss2*^{BATKO}. n=3 mice.

H. Rectal temperatures of the *Acss2*^{BATKO} male mice and littermate controls during cold exposure (4°C). n=5 C, 5 KO.

I. RT-PCR analysis of mitochondria and peroxisome FAO genes in BAT.**** p<0.0001, ***p=0.0001, ***p=0.0003, **p=0.0017, ****p<0.0001, ****p=<0.0001, *p=0.0268, ***p=0.0003. n=6–8 C, 6–8 KO. Ecl1, ehhadh, 2,4drc (n=6C, 6KO, mice batch 1); Cpt1a, Cpt1b, Pmp70, Cpt2, Cact, Crat (n=8C, 8KO, mice batch 2).

J. RT-PCR analysis of elongases. **p= 0.0035. n=6 C, 6 KO.

K. RT-PCR analysis of desaturases. **p=0.0049, *p=0.0120. n=6 C, 6 KO.

L. RT-PCR analysis of TG synthesis pathway genes.***p= 0.0004, **p=0.0016. n=6 C, 6 KO.

Data in panels C-F has been replicated 3 times.

Data are mean ± s.e.m. Statistical analysis unpaired two-tailed Student’s t-test.

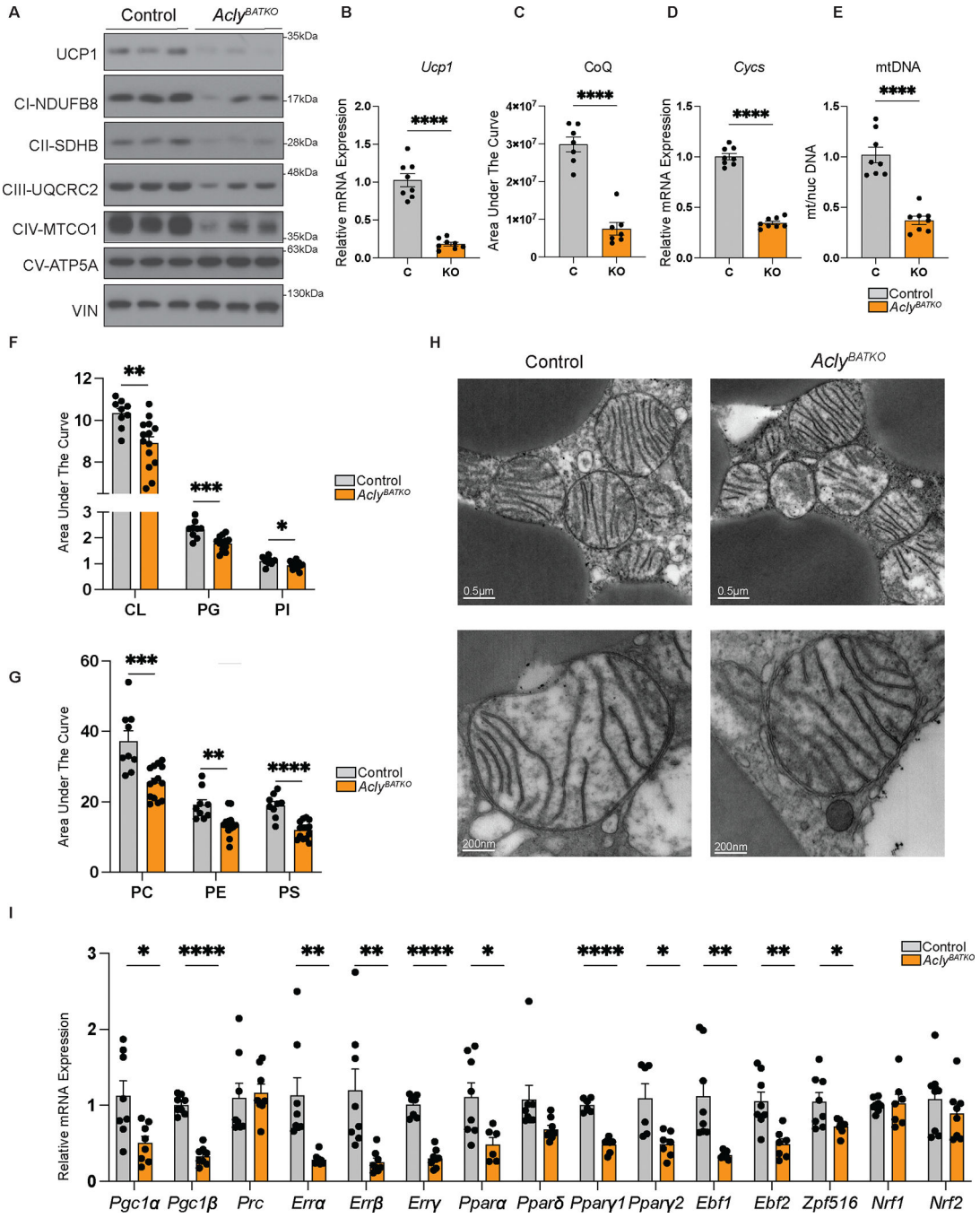

Fig. 2. The BAT Mitochondria Network and Thermogenic Program Requires ACLY.

A. Western blot of UCP1 and representative ETC proteins in BAT lysates prepared from control and *Acly*^{BATKO} mice.

B. RT-PCR analysis of *Ucp1* in BAT. ****p<0.0001. n=8 C, 8 KO.

C. CoQ levels in BAT. ****p<0.0001. n=7 C, 7 KO.

D. RT-PCR analysis of *Cycs* in BAT. ****p<0.0001. n=8 C, 8 KO.

E. BAT Mitochondria/Nuclear DNA ratio. ****p<0.0001. n=8 C, 8 KO.

F. Lipidomics analysis of cardiolipin (CL), phosphatidylglycerol (PG), phosphatidylinositol (PI) in BAT. **p=0.0036, ***p=0.0004, *p=0.0121.n=9 C, 14 KO.

G. Lipidomics analysis of phosphatidylcholine (PC), phosphatidylethanolamine (PE), phosphatidylserine (PS), in BAT. ***p=0.0004, **p=0.0019, ****p<0.0001. n=9 C, 14 KO.

H. Representative electron micrographs from the BAT of control and $Acly^{BATKO}$ mice; top: scale bar = 0.5um, bottom: scale bar = 200nm.

I. RT-PCR analysis of core thermogenic genes in BAT. *p=0.0111, ****p<0.0001, **p=0.0033, **p=0.0053, ****p<0.0001, *p=0.0181, ****p<0.0001, *p=0.0088, **p=0.0025, **p=0.0022, *p=0.0305. n=8 C, 8 KO.

Data are mean ± s.e.m. Statistical analysis unpaired two-tailed Student’s t-test.

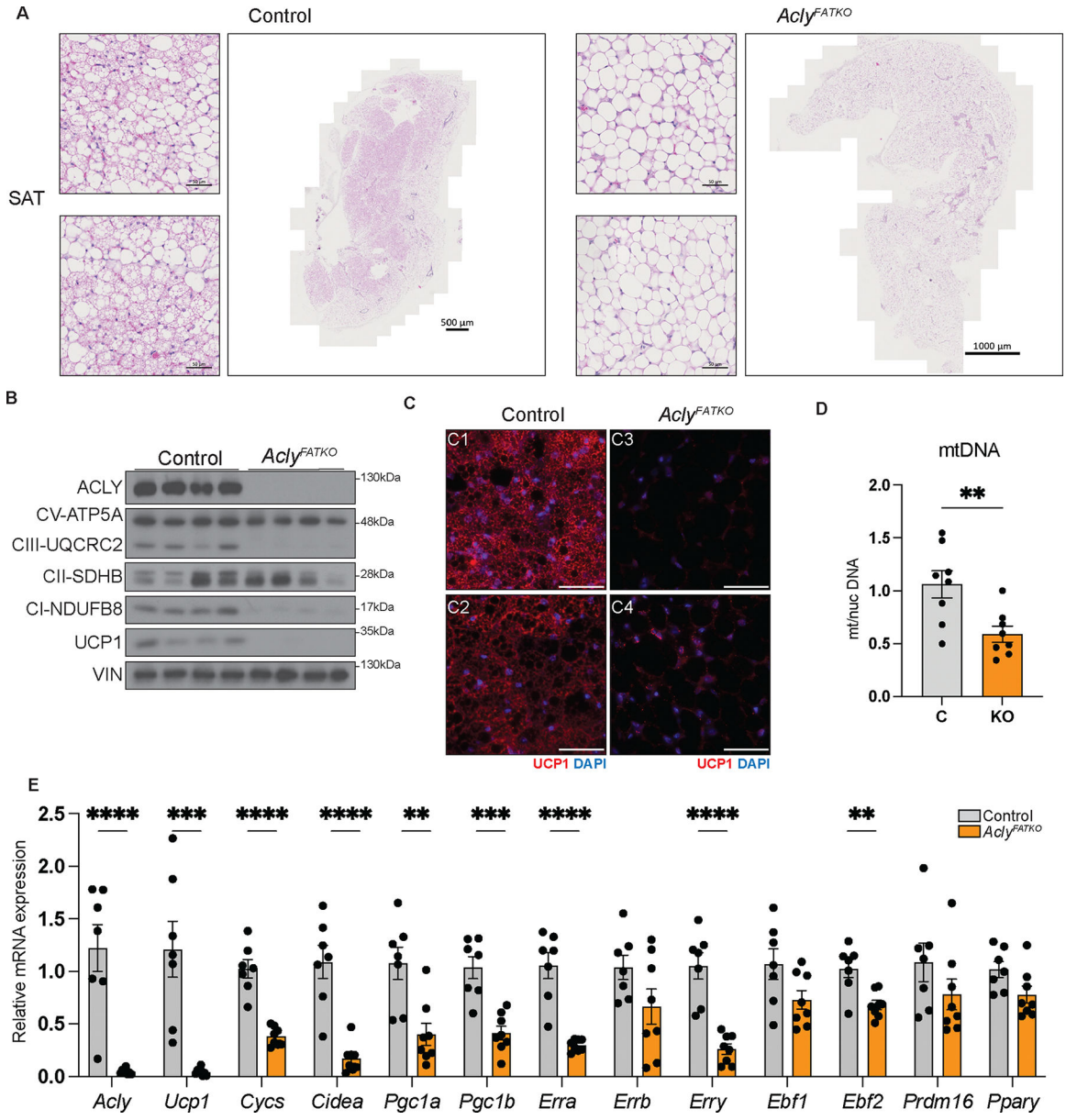

Fig. 3. Beige Adipocyte Formation Also Requires ACLY.

A. Representative H&E of the subcutaneous adipose tissue (SAT) from *Acly*^{FATKO} male mice and littermate controls housed at 6°C for 4 weeks. Top scale bars, left to right are 500uM and 1000uM. Bottom scale bars, 50um. Consistent result across n=5 animals.

B. Western blot of UCP1 and representative ETC proteins corresponding to (A). n=4mice.

C. Representative immunofluorescent staining of UCP1 and DAPI in the SAT from *Acly*^{FATKO} male mice (C3, C4) and littermate controls (C1, C2) housed at 6°C for 4 weeks. Scale bars, 50um.

D. Mitochondria/Nuclear DNA ratio in the SAT from *Acly*^{FATKO} male mice and littermate controls housed at 6°C for 4 weeks. **p=0.0070. n=8 C, 8 KO.

E. RT-PCR analysis of SAT from $Acly^{FATKO}$ male mice and littermate controls housed at 6°C for 4 weeks. ****p<0.0001, ***p=0.0004, ****p<0.0001, ****p<0.0001, **p=0.0026, ***p=0.0002, ****p<0.0001, ****p<0.0001, **p=0.0024 n=7 C, 8 KO.
Panels D: grey bar (Control), orange bar ($Acly^{FATKO}$).
Data are mean ± s.e.m. Statistical analysis unpaired two-tailed Student's t-test.

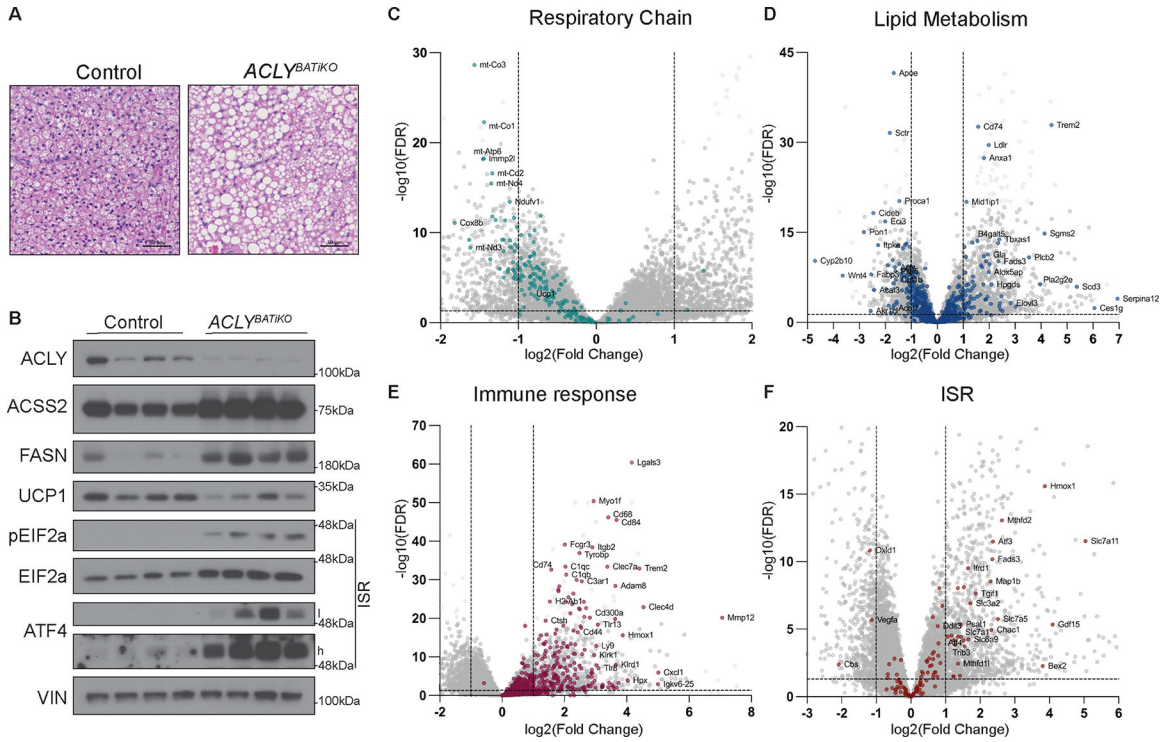

Fig. 4. Induced ACLY loss triggers the Integrated Stress Response.

A. Representative H&E of the BAT from *Acly*^{BATiKO} male mouse and littermate control. Scale bar 50um. Consistent result across n=3 mice.

B. Corresponding Western blot of the *Acly*^{BATiKO} male mice.

C-F. Volcano plots generated from bulk RNA-sequencing that show differential gene expression (log2(Fold Change) between control and induced *Acly* KO BAT for the following groups of genes:

C. Respiratory Chain genes.

D. Lipid Metabolism genes.

E. Immune Response genes.

F. Integrated stress response (ISR) genes.

Panels C-F are scaled to highlight specific pathways.

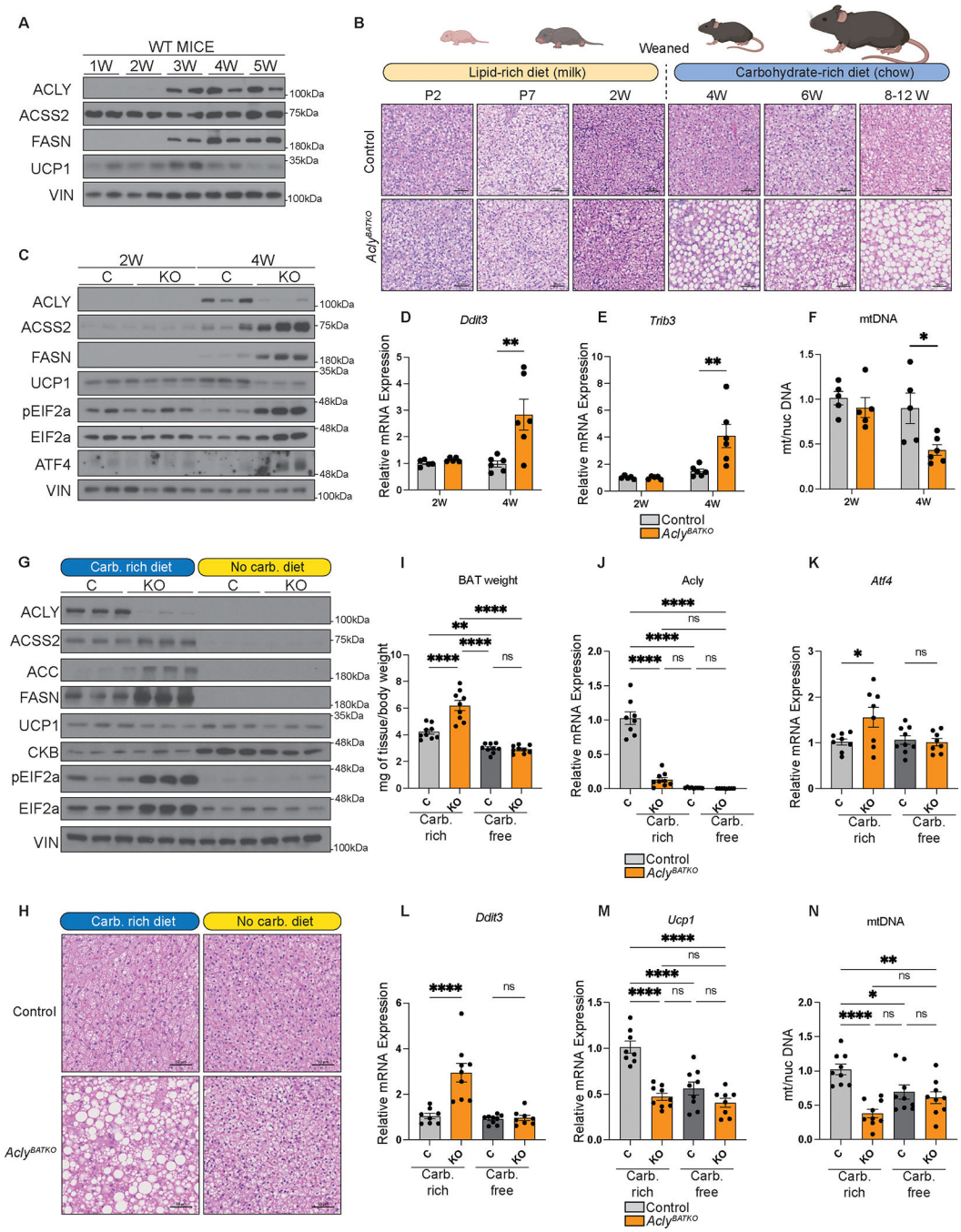

Fig. 5. ACLY's Role in Mitigating Stress is Linked to Dietary Carbohydrates.

A. Western blot form WT BAT lysates from 1- to 5-week-old mice weaned onto a standard laboratory diet. n=2 mice for each timepoint.

B. Representative H&E stains of BAT from *Acly*^{BATKO} mice and littermate controls from P2 to 8–12-week-old mice. Scale bar 50um. n=2 mice each timepoint. Created in BioRender. G, D. (n.d.) BioRender.com/q54z563.

C. Western blot of the iBAT from *Acly*^{BATKO} mice and littermate controls at 2 and 4 weeks of age.

D. RT-PCR analysis of *Ddit3* in the $Acly^{BATKO}$ mice 2 and 4 week of age. **p=0.0028. 2W: n=5 C, 5 KO; 4W: n=6 C, 6 KO.

E. RT-PCR analysis of *Trib3*. **p=0.0047. 2W: n=5 C, 5 KO; 4W: n=6 C, 6 KO.

F. Mitochondria/Nuclear DNA ratio in iBAT from $Acly^{BATKO}$ mice and littermate controls at 2 and 4 weeks of age. *p=0.0301. 2W: n=5 C, 5 KO; 4W: n=5 C, 6 KO.

G. Western blot of the iBAT from $Acly^{BATKO}$ mice and littermate controls on carb. rich or carb. free diet.

H. Representative H&E of the iBAT from $Acly^{BATKO}$ mice and littermate controls on carb. rich or carb. free diet. Scale bar 50um.

I. iBAT weight from $Acly^{BATKO}$ mice and littermate controls on carb. rich or carb. free diet. ****p<0.0001, **p=0.0023. Carb. rich: n=9 C, 9 KO; carb. free: n=9 C, 9 KO.

J. RT-PCR analysis of *Acly* in the iBAT from $Acly^{BATKO}$ mice and littermate controls on carb. rich or carb. free diet. ****p<0.0001. Carb. rich: n=8 C, 9 KO; carb. free: n=9 C, 8 KO.

K. RT-PCR analysis of *Atf4*. *p= 0.0319.

L. RT-PCR analysis of *Ddit3*. ****p< <0.0001.

M. RT-PCR analysis of *Ucp1*. ****p< <0.0001.

N. Mitochondria/Nuclear DNA ratio in iBAT from $Acly^{BATKO}$ mice and littermate controls on carb. rich or carb. free diet. ****p< <0.0001, *p= 0.0409, **p= 0.0070. Carb. rich: n=9 C, 9 KO; carb. free: n=9 C, 8 KO.

Panels I-N: grey bar (C) carb. rich diet, orange bar left ($Acly^{BATKO}$) carb.rich diet; dark grey bar (C) carb. free diet, orange bar right ($Acly^{BATKO}$) carb. free diet.

Data are mean ± s.e.m. Group differences determined via one-tailed ANOVA with Tukey's post hoc.

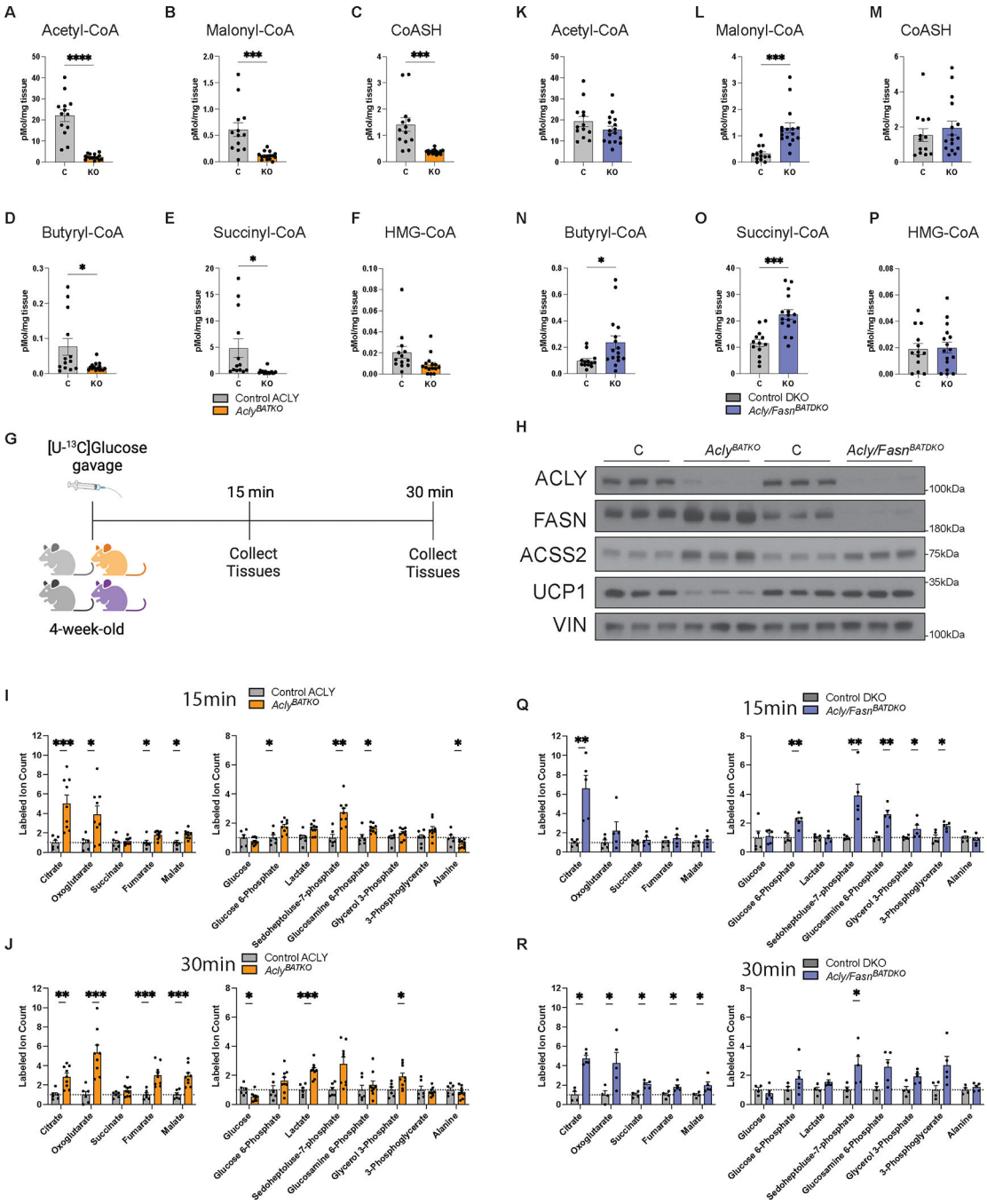

Fig. 6. ACLY Prevents TCA Cycle Overload During Thermogenesis.

A-F. Measurements of the indicated acly-CoA species in the BAT of control and *Acly*^{BATKO} mice. n=13 C, 15 KO.

A. Acetyl-CoA. ****p <0.0001.

B. Malonyl-CoA. ***p= 0.0004.

C. CoASH. ***p= 0.0002.

D. Butyryl-CoA. *p= 0.0165.

E. Succinyl-CoA. *p= 0.0105.

F. HMG-CoA.

G. Schematic of [U-^{13}C]Glucose tracing experiment.

H. Western blot of the *Acly*^{BATKO} and *Acly,Fasn*^{BATKO} male mice. n=3 mice for each condition.

I-J. Labeled ion counts for metabolites in the *Acly*^{BATKO} mice BAT at 15 minutes (I) and 30 minutes (J). 15min: Left ***p= 4e-04, *p= 0.0256, *p= 0.0176, *p= 0.012.Right *p= 0.0176, **p= 0.00759, *p= 0.0176, *p= 0.0256. n=6C, 9 KO.

30min:Left **p= 0.0016, ***p= 4e-04, ***p= 4e-04, ***p= 4e-04. Right *p= 0.012, ***p= 4e-04, *p= 0.036.

K-P. Measurements of the indicated acly-CoA species in the BAT of control and *Acly,Fasn*^{BATKO} mice. n=13 C, 16 KO.

K. Acetyl-CoA.

L. Malonyl-CoA. ***p= 0.0001.

M. CoASH.

N. Butyryl-CoA. *p= 0.0226.

O. Succinyl-CoA.***p= 0.0001.

P. HMG-CoA.

Q-R. Labeled ion counts for metabolites in the *Acly,Fasn*^{BATKO} mice BAT at 15 minutes (Q) and 30 minutes (R). n=4C, 5 KO. 15min:Left **p= 0.00794. Right **p= 0.00794, **p= 0.00794, **p= 0.00794, *p= 0.0317, *p= 0.0159.

30min:Left *p= 0.0159, *p= 0.0317, *p= 0.0159, *p= 0.0159, *p= 0.0159. Right *p= 0.0317.

Panels I, J, Q, R: Statistical analysis is two-sample Wilcoxon.

Data are mean ± s.e.m. Group differences determined via one-tailed ANOVA with Tukey's post hoc.

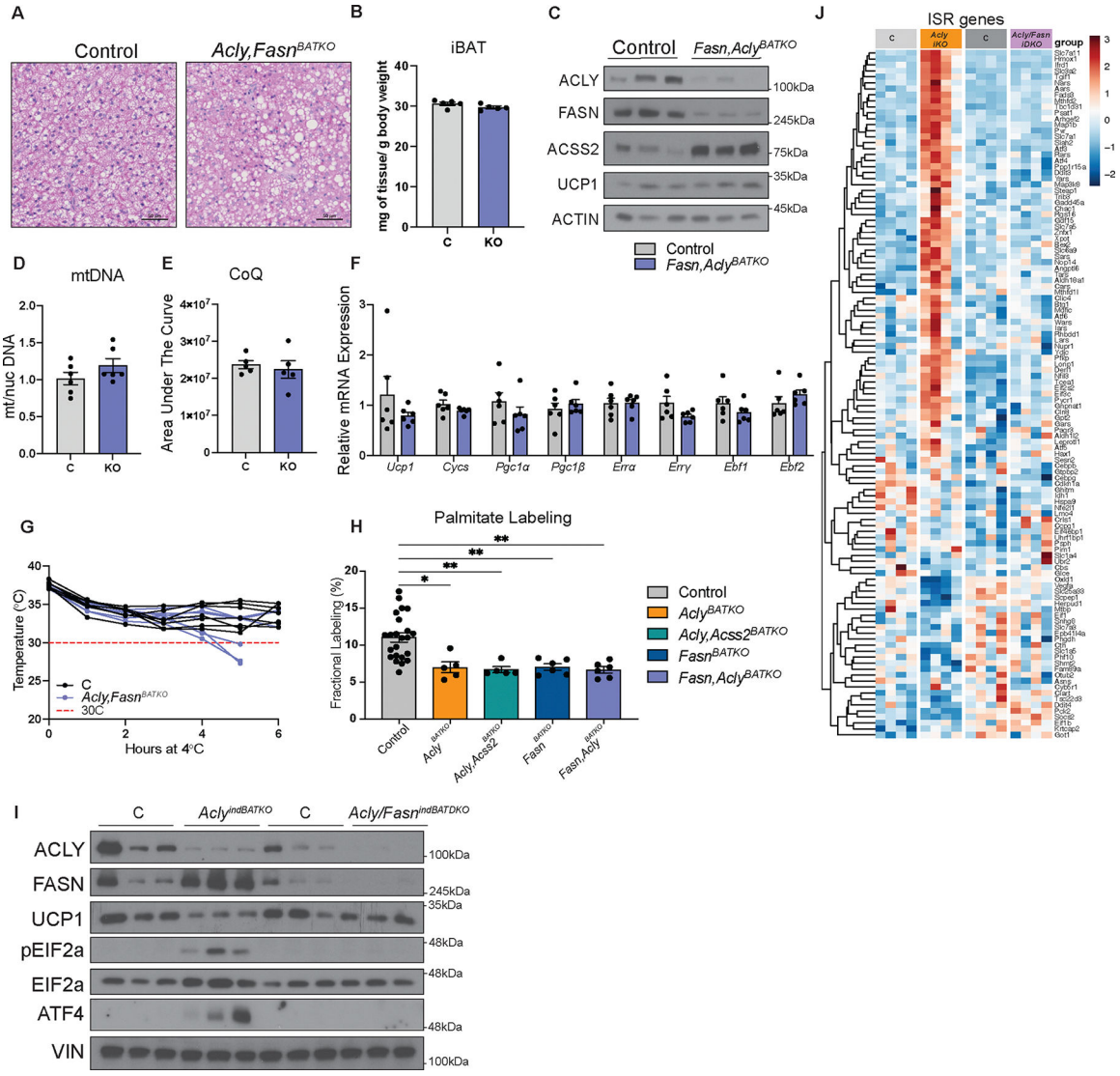

Fig. 7. BAT *Acly;Fasn* Double Knockout Rescues Thermogenesis Independent of DNL and Prevents ISR.

A. Representative H&E of the iBAT from Fasn,AclyBATKO male mouse and littermate control. Scale bar 50um. Consistent in n=4 mice.

B. Tissue weights (iBAT) from Fasn,AclyBATKO mice and littermate controls. n=5 C, 5 KO.

C. Western blot of the Fasn,AclyBATKO.

D. Mitochondria/Nuclear DNA ratio in iBAT from Fasn,AclyBATKO mice and littermate controls. n=6 C, 6 KO.

E. CoQ levels in the Fasn,AclyBATKO mice BAT. n=5 C, 5 KO.

F. RT-PCR analysis the iBAT from Fasn,AclyBATKO mice and littermate controls. n=6 C, 6 KO.

G. Rectal temperatures of the Fasn,AclyBATKO male mice and littermate controls during cold exposure (4°C). n=7 C, 7 KO.

H. D2O labeling of newly synthesized palmitate in the AclyBATKO(n=5,*p= 0.0109), Acly;Acss2BATKO(n=5,**p= 0.0053), FasnBATKO(n=6,**p= 0.0068), Fasn;AclyBATKO(n=6,**p= 0.0022) mice BAT and their littermates(n=23).
I. Western blot of the AclyBATiKO and Fasn,AclyBATiKO BAT. n=3 mice each condition.
J. Heat map relative abundance of ISR genes in RNAseq of AclyBATiKO and Fasn,AclyBATiKO BAT.
Data are mean ± s.e.m. Statistical analysis unpaired two-tailed Student’s t-test. Group differences determined via one-tailed ANOVA with Tukey’s post hoc.

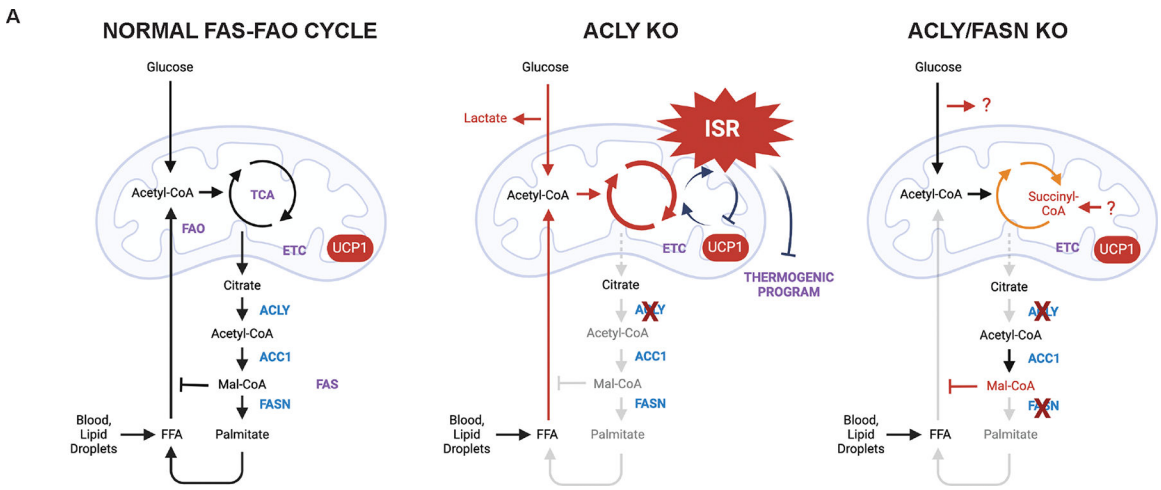

Fig. 8. Model of futile FAS-FAO cycling in BAT and the role of ACLY and FASN.

(left) Depiction of normal futile FAS-FAO cycling in active BAT. (middle) ACLY is essential for FAS-FAO cycling in the BAT of mildly cold mice, where it promotes citrate efflux from mitochondria and into *de novo* lipid synthesis to reduce pressure on the TCA cycle and facilitate efficient metabolic flux. In the absence of ACLY, increased carbon flux into the mitochondria from both FFAs and glucose causes TCA cycle overload which activates the integrated stress response and downregulates UCP1 expression. Loss of UCP1 may additionally or independently cause further mitochondrial stress. (right). Doubly deleting *Acly* and *Fasn* restores metabolic homeostasis by unlocking an alternative metabolic program defined by higher-than-normal malonyl-CoA. Because ACLY is deficient in this context, the high malonyl-CoA must be generated from an alternative source of acetyl-CoA, and the high malonyl-CoA levels would depressurize the TCA cycle by attenuating flux from FAO through its classic mechanism of allosterically inhibiting fatty acid uptake into mitochondria (via CTP1). High succinyl-CoA levels and altered glucose flux in the double knockout BAT suggests additional metabolic reprogramming steps may also help reestablish homeostasis. Created in BioRender. G, D. (2024) BioRender.com/h38h345.

Primer sequences.

qPCR Primers		
Gene name	**Forward Sequence**	**Reverse Sequence**
Cpt1a	GACCCTAGACACCACTGGCCG	GAGAAGACCTTGACCATAGCC
Cpt1b	GCACACCAGGCAGTAGCTTT	CAGGAGTTGATTCCAGACAGGTA
Cpt2	CAGCACAGCATCGTACCCA	TCCCAATGCCGTTCTCAAAAT
Cact	GACGAGCCGAAACCCATCAG	AGTCGGACCTTGACCGTGT
Crat	GCTGCCAGAACCGTGGTAAA	CCTTGAGGTAATAGTCCAGGGA
Ecl1	ACTGGAAGAACGTGCAGGAG	AAACCAGAAGGGGGCAACAA
Pmp70	GGCCTGCACGGTAAGAAAAGT	CCGCAATAAGTAACAAGTAGCCT
Ehhadh	ATGATCCGCCTCTGCAATCC	GCTCCACAGATCACTATGGCT
2,4drc	TCATCGTCGGCAGGAGTCTG	CATGACCTCTGGGGGAACTC
Elovl1	GTGGCCCAGCCCTACCTT	TGTGCAGTGAGACCAGGACAA
Elovl3	ATGAATTTCTCACGCGGGTTA	GAGCTTACCCAGTACTCCTCCAAA
Elovl4	GTGGGTGGCTGGAGGCCAAGCGTTTTT	ATTCGTGGCCGTCTTTCCGGTTTTTGA
Elovl6	TCAGCAAAGCACCCGAAC	AGCGACCATGTCTTTGTAGGAG
Dgat1	GAGGCCTCTCTGCCCCTATG	GCCCCTGGACAACACAGACT
Dgat2	CCGCAAAGGCTTTGTGAAG	GGAATAAGTGGGAACCAGATCA
Agpat1	GCTGGCTGGCAGGAATCAT	GTCTGAGCCACCTCGGACAT
Scd1	CCCTGCGGATCTTCCTTATC	TGTGTTTCTGAGAACTTGTGGTG
Sc5d	CCAAATGGCTGGATTCATCT	GTCCACAGGGTGAAAAGCAT
Ucp1	CTGCCAGGACAGTACCCAAG	TCAGCTGTTCAAAGCACACA
Cycs	CCAAATCTCCACGGTCTGTTC	ATCAGGGTATCCTCTCCCCAG
Pgc1a	TATGGAGTGACATAGAGTGTGCT	CCACTTCAATCCACCCAGAAAG
Pgc1b	TCCTGTAAAAGCCCGGAGTAT	GCTCTGGTAGGGGCAGTGA
Prc	CAGGAGAAGAAGCCCTTAGACC	CTTTCGCCAAGAGTGAGACAG
Erra	CTCAGCTCTCTACCAAACGC	CCGCTTGGTGATCTCACACTC
Errb	ATGCGAGTACATGCTTAACGC	CATCCCCACTTTGAGGCATTT
Erry	AAGATCGACACATTGATTCCAGC	CATGGTTGAACTGTAACTCCCAC
Ppara	GACATGGAGACCTTGTGTATGG	AGGAACTCGCGTGTGATAAAG
Ppard	TCCATCGTCAACAAAGACGGG	ACTTGGGCTCAATGATGTCAC
Ppary1	TGAAAGAAGCGGTGAACCACTG	TGGCATCTCTGTGTCAACCATG
Ppary2	GCATGGTGCCTTCGCTGA	TGGCATCTCTGTGTCAACCATG
Ebf1	GCATCCAACGGAGTGGAAG	GATTTCCGCAGGTTAGAAGGC
Ebf2	GGGATTCAAGATACGCTAGGAAG	GGAGGTTGCTTTTCAAAATGGG
Zpf516	ACCGGACAGGAACTCTGATTC	GAGGTGCTCTTAGTAGGGCTG
Nrf1	AGCACGGAGTGACCCAAAC	TGTACGTGGCTACATGGACCT
Nrf2	TAGATGACCATGAGTCGCTTGC	GCCAAACTTGCTCCATGTCC
Acly	CTCACACGGAAGCTCATCAA	ACGCCCTCATAGACACCATC

qPCR Primers		
Gene name	**Forward Sequence**	**Reverse Sequence**
Cidea	ATCACAACTGGCCTGGTTACG	TACTACCCGGTGTCCATTTCT
Prdm16	GACATTCCAATCCCACCAGA	CACCTCTGTATCCGTCAGCA
Ddit3	GCAGCGACAGAGCCAGAATAA	TGTGGTGGTGTATGAAGATGCA
Trib3	CTTGCGCGACCTCAAGCT	ATCACGCAGGCATCTTCCA
Atf4	CTCGGAATGGCCGGCTAT	GTCCCGGAAAAGGCATCCT
Glut1	GCTGTGCTTATGGGCTTCTC	AGAGGCCACAAGTCTGCAT
Glut4	GTGACTGGAACACTGGTCCTA	CCAGCCAGTTGCATTGTAG
Cd36	TGGCCTTACTTGGGATTGG	CCAGTGTATATGGCTCATCCA
Lpl	GGCCAGATTCATCAACTGGAT	GCTCCAAGGCTGTACCCTAAG
Chac1	GGCTTCGTTCGTGGCTATAGC	CAGCCCTCACGGTCTTCAAG
Acss2	GCTTCTTTCCCATTCTTCGGT	CCCGGACTCATTCAGGATTG
Fasn	GCTGCGGAAACTTCAGGAAAT	AGAGACGTGTCACTCCTGGACTT
Chrebpa	CGACACTCACCCACCTCTTC	TTGTTCAGCCGGATCTTGTC
Chrebpb	TCTGCAGATCGCGTGGAG	CTTGTCCCGGCATAGCAAC
Actin	ATGGAATCCTGTGGCATCCA	CGCTCAGGAGGAGCAATGAT
Tbp	ACGGACAACTGCGTTGATTTT	ACTTAGCTGGGAAGCCCAAC
mthNA Primers		
Gene name	**Forward Sequence**	**Reverse Sequence**
ND1	CTAGCAGAAACAAACCGGGC	CCGGCTGCGTATTCTACGTT
HK2	GCCAGCCTCTCCTGATTTTAGTGT	GGGAACACAAAAGACCTCTTCTGG

Table 2:

GO Terms for Figures 4(C–F), 7(J), and Ext. Fig. 10(H).

Respiratory Chain	GO:1901857, GO:0045333, GO:0022900, GO:0022904, GO:0042775, GO:0019646, GO:0042773, GO:0006120, GO:0043457, GO:0006123, GO:0006122, GO:1901856
Immune Response	GO:0002764, GO:0045088, GO:0002757, GO:0045089, GO:0002218, GO:0002758, GO:0002768, GO:0002429, GO:0002697, GO:0002263, GO:0002366, GO:0002699, GO:0002285, GO:0002700, GO:0002520, GO:0002819, GO:0002440, GO:0050777, GO:0002702, GO:0002460, GO:0002822, GO:0002821, GO:0002224, GO:0002367, GO:0002220, GO:0002718, GO:0045824, GO:0002824, GO:0002312, GO:0002720, GO:0140895, GO:0002200, GO:0002562, GO:0002286, GO:0002698, GO:0002381, GO:0002287, GO:0002292, GO:0042088, GO:0002275, GO:0002293, GO:0140894, GO:0002294, GO:0034142, GO:0034121, GO:0061081, GO:0002204, GO:0002208, GO:0002825, GO:0061760, GO:0002755, GO:0072538, GO:0002889, GO:0034122, GO:0034162, GO:0140374, GO:0002827, GO:0002891, GO:0002283, GO:0002313, GO:0042092, GO:2000316, GO:0002281, GO:2000318, GO:0002701, GO:0002756, GO:0034138, GO:0002828, GO:0034154, GO:0016064, GO:0034163, GO:0034134, GO:0033006, GO:0002279, GO:0002820, GO:0002823, GO:0034143, GO:0002719, GO:0034135, GO:0002455, GO:0002829, GO:0002830, GO:0033007, GO:0002423
Lipid Metabolism	GO:0046486, GO:0006644, GO:0006650, GO:0006665, GO:0006643, GO:0019216, GO:0045833, GO:0006687, GO:0006631, GO:0019395, GO:0034440, GO:0006644, GO:0046486, GO:0006631, GO:0006650, GO:0019216, GO:0045834, GO:0046320, GO:0006638, GO:0019217, GO:0006664, GO:0006643, GO:0046459, GO:0046322, GO:0045833, GO:0045922, GO:0000038, GO:0046321, GO:1903725, GO:0045923, GO:0006665, GO:0006687
ISR	ISR signature gene transcripts (Han et al., 2023)